Enhancing the Magnetization Blocking Energy of Biradical-Metal System by Merging Discrete Complexes into One-Dimensional Chains

Junfang Xie, Jing Han, Xiaohui Huang, Chaoyi Jin, Licun Li, Jean-pascal Sutter

Enhancing the Magnetization Blocking Energy of Biradical-Metal System by Merging Discrete Complexes into One-Dimensional Chains

Junfang Xie,[a] Jing Han,[a] Xiaohui Huang,[a] Chaoyi Jin,[a] Licun Li*[a] and Jean-Pascal Sutter*[b]

[a] J.-F. Xie, J. Han, X.-H. Huang, C.-Y. Jin, Prof. L.-C. Li
Department of Chemistry, Key Laboratory of Advanced Energy Materials Chemistry, College of Chemistry, Nankai University, Tianjin 300071, China
Email: llicun@nankai.edu.cn

[b] Dr. J.-P. Sutter
Laboratoire de Chimie de Coordination du CNRS (LCC-CNRS), Université de Toulouse, CNRS, Toulouse, France
Email: jean-pascal.sutter@lcc-toulouse.fr

Abstract: The reaction of nitronyl nitroxide biradical NITPhMeImbis [5-(2-methylimidazole)-1,3-bis(1′-oxyl-3′-oxido-4′,4′,5′,5′-tetramethyl-4,5-hydro-1*H*-imidazol-2-yl)-benzene] with $Ln(hfac)_3 \cdot 2H_2O$ and $Cu(hfac)_2$ (hfac = hexafluoroacetylacetonate), led to two series of 2*p*-3*d*-4*f* complexes, namely, nona-spin clusters, $[Ln_2Cu_3(hfac)_{12}(NITPhMeImbis)_2]$ (Ln = Gd **1,** Dy **2**), or one-dimensional chains $[LnCu_2(hfac)_7(NITPhMeImbis)]$ (Ln = Y **3,** Dy **4,** Tb **5**) depending on the temperature of the reaction. All five complexes contain a biradical-Ln unit in which the biradical chelates the Ln^{III} ion by the means of one aminoxyl (i.e. NO) group of each NIT unit. For the discrete complexes, a $Cu(hfac)_2$ links two biradical-Ln units via one of the remaining NO groups, while for the chain compounds, the two remaining NO groups of the biradical-Ln moiety are each coordinated to a $Cu(hfac)_2$ unit to form a 1D coordination polymer. Moreover, a terminal $Cu(hfac)_2$ unit is coordinated to the imidazole-N atom of the NITPhMeImbis ligand. Spin dynamics investigations evidenced the onset of slow relaxation of the magnetization for **2**, whereas **4** and **5** exhibit a typical single-chain magnet behavior. This highlights the vital role of the 1D spin correlation in the blocking of the magnetization. These results illustrate that from the same basic building blocks, magnetic relaxation can be carefully modulated by structural adjustments.

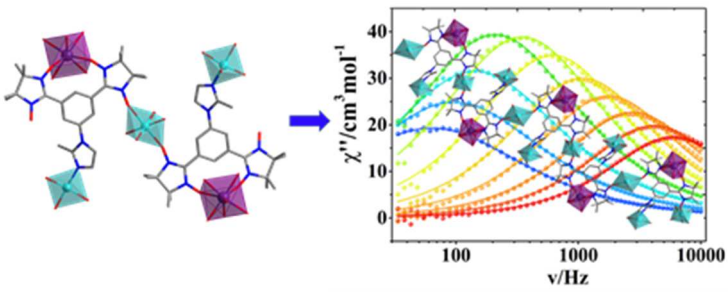

Keywords: 2*p*-3*d*-4*f* • nitronyl nitroxide biradical • magnetic properties • SCMs • structural transformation

Introduction

The assembly of anisotropic metal ions with radical ligands is a promising synthesis strategy for the construction of molecular nanomagnets,[1] *i.e.* single-molecule magnets (SMMs)[2] and single-chain magnets (SCMs),[3] which have potential applications in the fields of high-density information storage, molecular spintronics, and quantum computing.[4] A prominent example of SMMs is a di-Tb complex bridged by a N_2^{3-} radical that exhibits a blocking of its magnetization up to T_B = 20 K.[5] More recently, a series of dilanthanidofullerene compounds[6] connected by an unpaired electron acting as a paramagnetic linker were shown to exhibit remarkable magnetic relaxation behaviors, as exemplified by $Tb_2@C_{80}(CH_2Ph)$ showing a T_B near 30 K.[7] In the area of SCMs, the seminal example was a 1D polymer consisting in nitronyl nitroxide radical (NIT) and $Co(hfac)_2$, $[Co(hfac)_2(NITPhOMe)]$ (hfac = hexafluoroacetylacetonate).[3a] Subsequently, a series of Co(II)-nitronyl nitroxide chains exhibiting coercive fields as large as 6 T have been reported.[3b, 3c, 8] Compared to SMMs, SCMs are anticipated to possess a higher energy barrier for magnetization reversal due to the additional correlation energy (Δ_ξ), which stems from the exchange interactions (J) between the spin carriers along the chain.[9] Recently, Houard and coworkers achieved chiral supramolecular nanotubes SCMs supported by a nitronyl nitroxide radical substituted with an aliphatic chain.[10] However, the design and the elaboration of SCMs remain challenging.

Most of reported radical-based SCMs involve either 3*d* or 4*f* metal ions, but recently, gathering 3*d* and 4*f* ions in association with radical ligands, 2*p*-3*d*-4*f* chains emerged as a new strategy for designing SCMs.[1d, 11] The nitronyl nitroxide radical can act as a bridging ligand to coordinate to both transition metal and lanthanide ions, leading to strong magnetic exchange interactions. These remarkable characteristics make this radical ligand ideally suited for the design of SCMs and for exploring the potential offered by three different spin carriers to increase the blocking temperatures. Some interesting 2*p*-3*d*-4*f* chains with SCM behavior have been reported.[12] A notable advance has been achieved through the use of ferromagnetic nitronyl nitroxide diradicals. This reduced the effect of the next-neighbor radical-radical antiferromagnetic interaction mediated by the Ln center, which competes with ferromagnetic Ln-Radical interaction. As a result, larger energy barriers for the magnetic relaxation were obtained.[13]

Inspired by these results and with the aim of further probing nitronyl nitroxide biradical bridged *d-f* heterometallic chains, a series of investigations were conducted with the novel nitronyl nitroxide biradical NITPhMeImbis [i.e. 5-(2-methylimidazole)-1,3-bis(1′-oxyl-3′- oxido-4′,4′,5′,5′-tetramethyl-4,5-hydro-1*H*- imidazol-2-yl)-benzene; Scheme 1]. Herein we disclose two families of 2*p*-3*d*-4*f* complexes, namely, nona-spin clusters of formula $[Ln_2Cu_3(hfac)_{12}(NITPhMeImbis)_2]$ (Ln = Gd **1**, Dy **2**; hfac = hexafluoroacetylacetonate) and the chain homologues $[LnCu_2(hfac)_7(NITPhMeImbis)]$ (Ln = Y **3**, Dy **4**, Tb **5**). Interestingly, the former can be deemed as a discrete unit of the latter. Magnetic studies revealed SCM behavior for **4** and **5** whereas only the onset of slow relaxation of the magnetization was observed for **2** at low *T*.

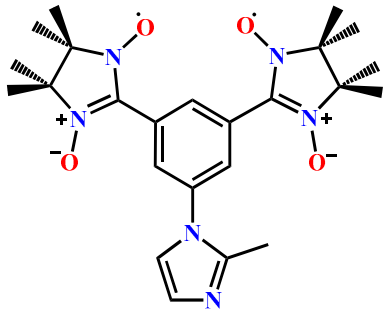

Scheme 1. The biradical ligand NITPhMeImbis

Results and Discussion

Synthesis

With the purpose to construct new 2*p*-3*d*-4*f* chains, the new NITPhMeImbis biradical was reacted with $Ln(hfac)_3.2H_2O$ and $Cu(hfac)_2$ in 1:1:2 ratio. We found that the temperature at which the reaction was performed had a critical effect on the outcome. A pentanuclear complex (i.e. **1**, **2**) was obtained when the reaction was performed at about 80°C, whereas the 1D assemblage (**3**-**5**) was achieved at the boiling point of *n*-heptane. Accordingly, the reaction appears to be under thermodynamic control.

PXRD experiments confirmed the excellent phase purity of all crystalline samples (Figure S11).

Crystal Structures

Crystal structures obtained from single-crystal X-ray diffraction studies confirmed that complexes **1** and **2** are isostructural pentanuclear complexes (Figure 1 and S1). For the sake of brevity, only the structure of the Dy derivative is described, details regarding **1** can be found in the SI.

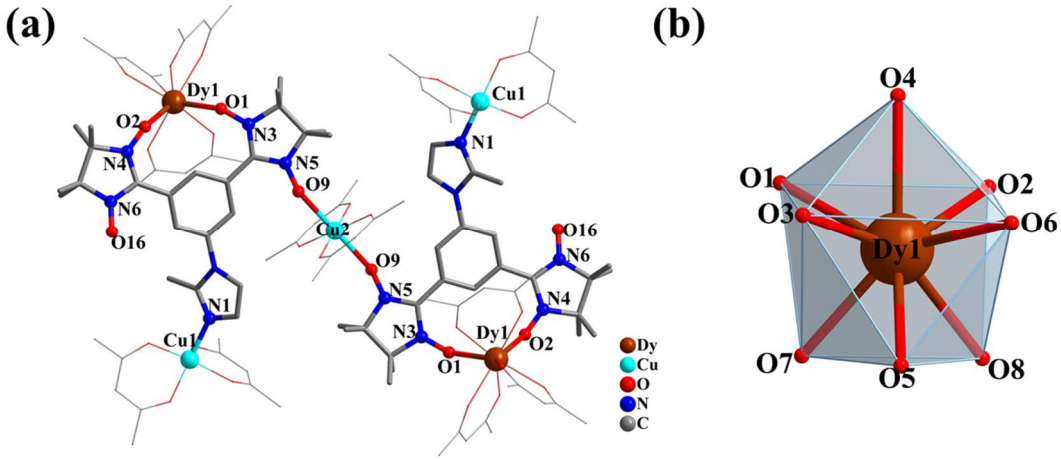

Figure 1. (a) Molecular structure of the pentanuclear complex **2** (H and F atoms are omitted for clarity.). (b) The coordination polyhedron of the Dy^{III} ion

The compound consists of two NITPhMeImbis ligands, two [Ln(hfac)$_3$] and three [Cu(hfac)$_2$] units (Figure 1). Each ligand chelates a Ln^{III} ion by the means of one aminoxyl (i.e. NO) group of each NIT unit to form a Ln-biradical unit, and the N atom on methylimidazole moiety coordinates a terminal [Cu(hfac)$_2$]. Two such Ln-biradical units are coordinated in *trans* position to a further Cu(hfac)$_2$ via one of their remaining NO groups, thus forming a symmetrical pentanuclear complex. In this organization, the eight-coordinated environment of Dy^{III} is completed by three bidentate β-diketonate anions (Dy-O_{hfac}: 2.301(5)-2.368(5) Å). Continuous Shape Measures (CShM, SHAPE software)[14] analysis indicates that the local symmetry around the Dy^{III} is C_{2v}, corresponding to a coordination polyhedron with a distorted biaugmented trigonal prism geometry (Table S3). The Dy-O_{rad} distances, 2.328(4) and 2.453(4) Å, are comparable to the Dy–O(rad) distances of related complexes reported in the literature.[2a, 15] The O_{rad}-Dy-O_{rad} angle is 84.19(2)° and the Dy-O-N-C torsion angles are -72.31(9)° and 63.94(8)°, respectively. The dihedral angles between the ON-C-NO plane of a NIT and the benzene ring are 25.77(8)° and 20.68(5)°, respectively. The coordination sphere of the terminal copper (Cu1) displays a distorted pyramidal geometry in which the basal sites are occupied by one N atom from methylimidazole (Cu1-N: 1.962(5) Å) and three O atoms from two $hfac^-$ ions (Cu-O_{hfac}: 1.934(4)–1.964(4) Å); the remaining O_{hfac} atom is located in axial position (Cu-O_{hfac}: 2.206(4) Å). The latter long bond is due to the *Jahn-Teller* effect. The Cu1-Dy1 distance is 10.592(1) Å. The *Jahn-Teller* effect also acts on Cu2, which displays an elongated octahedral coordination sphere. Two NO groups from two different NITPhMeImbis ligands are in the apical

positions (Cu-O_{rad}: 2.512(4) Å), and four O atoms from two hfac ligands are located in the equatorial positions (Cu-O_{hfac}: 1.928(4)-1.933(4) Å). The Dy1···Cu2 distance through the NIT moiety is 8.453(6) Å. The packing diagram of **2** (Figure S4) indicates that the shortest intermolecular Dy···Dy and Dy···Cu separations are 10.033(7) Å and 8.453(6) Å, respectively. The closest distance between non-coordinated aminoxyl groups is 7.188(7) Å.

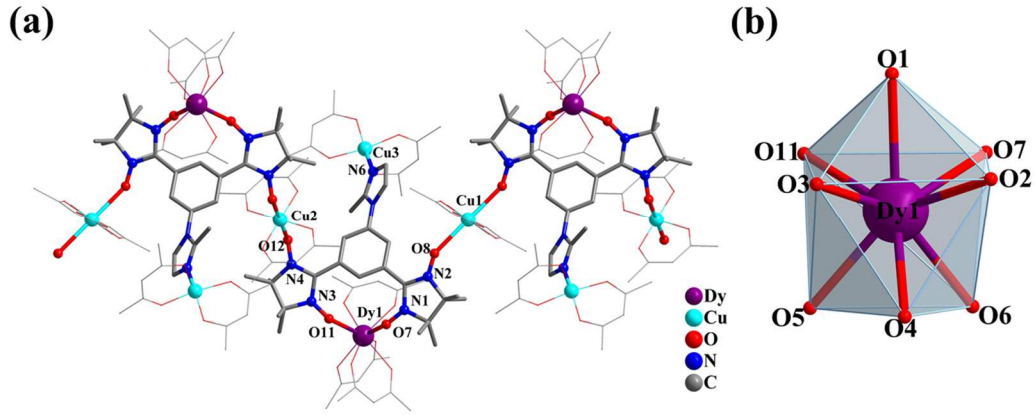

Figure 2. (a) One-dimensional structure of **4** (H and F atoms are omitted for clarity.). (b) The coordination polyhedron of the Dy^{III} ion.

Complexes **3-5** crystallized in the triclinic *P*$\bar{1}$ space group and have isomorphic chain structure (Figures 2 and S5-6). Complex **4** is described as the representative, information about **3** and **5** can be found in the SI. The asymmetric unit of complex **4** consists of one NITPhMeImbis, one $Dy(hfac)_3$ and two $Cu(hfac)_2$ units. As for the pentanuclear derivatives, each NITPhMeImbis chelates a Dy^{III} ion through its two neighboring NO groups but in **4** the remaining two aminoxyl (NO) moieties are coordinated to copper ions Cu1 and Cu2 respectively. Each of these Cu ions is further linked to the NO of another NITPhMeImbis to form one-dimensional compound. Cu1 and Cu2 exhibit an elongated octahedral CuO_6 coordination sphere, in which the axial positions are occupied by O atoms from two NO groups (Cu-O_{rad}: 2.453(9)-2.526(8)Å) and the other four O atoms from two hfac coligands are situated in the equatorial sites (Cu-O_{hfac}: 1.929(7)-1.938(1) Å). The N atom of methylimidazole group coordinates with a terminal Cu ion (Cu3). This displays a square pyramidal coordination sphere in which one O_{hfac} atom is located in axial position (Cu3-O_{hfac}: 2.187(9) Å), and the other three O_{hfac} atoms and one N atom from the methylimidazole ring site in the basal positions (Cu3-O_{hfac}: 1.919(9)-1.956(8) Å; Cu3-N:1.985(8) Å). The Dy^{III} ion is connected to the two nitroxides units of NITPhMeImbis ligand by the means of an oxygen atom from the NO moieties

(Dy-O_{rad}: 2.386(6), 2.348(7) Å) and to three hfac anions (Dy-O_{hfac}: 2.298(7)-2.361(7) Å). These bond lengths are close to those found in compound **2**. SHAPE analysis[14] indicates the Dy^{III} ion holds biaugmented trigonal prism (C_{2v}) coordination sphere (Table S3). The Dy-O-N-C torsion angles are 66.18(1)° and -68.81(2)°, respectively, and the O_{rad}-Dy-O_{rad} bond angle is 82.22(2)°. The dihedral angles between the ON-C-NO moieties and the phenyl ring of the NITPhMeImbis are 28.23(5)° and 27.14(5)°, which are slightly larger than those in **2**. The intra-chain Dy···Cu distances are 8.666(8) Å for Cu1 and 8.265(8) Å for Cu2. Packing arrangements are show in Figures S8-S10. The shortest inter-chain Dy···Dy and Dy···Cu separations are 11.657(1) Å and 8.337(2) Å, respectively.

Static magnetic properties

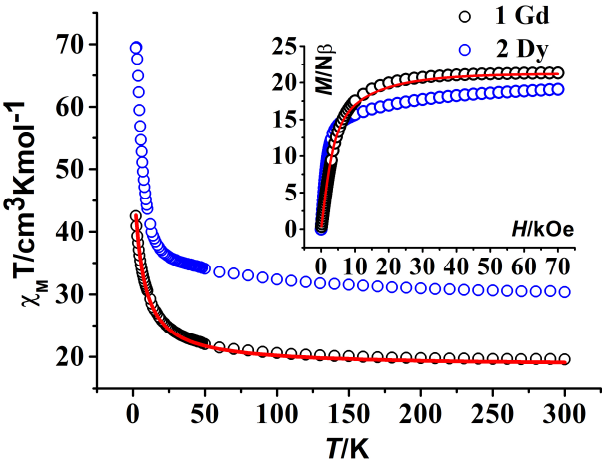

Figure 3. Plots of $\chi_M T$ versus T for **1** and **2**. Inset: Field-dependent magnetization for **1** and **2** (2.0K). The red line is the behavior calculated by *PHI*.

Variable-temperature magnetic susceptibilities for two series of compounds were obtained in a field of 1000 Oe between 2 and 300 K.

For complex **1** (Figure 3), the $\chi_M T$ value at room temperature is 19.58 cm^3 K mol^{-1}, which is slightly larger than the expected 18.39 cm^3 K mol^{-1} for the Curie contributions of two Gd^{III} ions ($^8S_{7/2}$, g = 2, C = 7.88cm^3 K mol^{-1}), three Cu^{II} ions (S = 1/2, g = 2, C = 0.375 cm^3 K mol^{-1}) and four radicals (S = 1/2, g = 2, C = 0.375 cm^3 K mol^{-1}). With lowering temperature, the value of $\chi_M T$ progressively raises to 42.50 cm^3 K mol^{-1} for 2 K. Such a behavior indicates that ferromagnetic interactions prevail in **1**. The field dependence of the magnetization recorded at 2 K (Figure 3) shows a fast increase for low fields before saturating above 20 kOe. The value of 21.33 $N\beta$ reached for 70 kOe is consistent with expected saturation value of 21 $N\beta$. Making reference to the crystal

structure, complex **1** can be described as a linear [rad-Gd-rad-Cu-rad-Gd-rad] magnetic unit plus two isolated Cu^{II} ions. Indeed, the magnetic interaction between Cu^{II} and radical groups through benzene and iminazole moiety must be very weak and can be ignored. Therefore, the magnetic exchanges scheme in this system consists of three kinds of communication paths (Scheme 2), namely, (i) the Gd^{III}-NO interaction (J_1), (ii) the interaction between Cu^{II} and the axial coordinated nitroxide group (J_2) and (iii) the combined NIT-NIT interaction via Gd^{III} ion and benzene ring (J_3). For the present nine-spin system, simultaneously fitting of the $\chi_M T$ and magnetization data was obtained with the PHI program[16] based on the following Hamiltonian (equation 1) plus two independent Cu centers ($S = ½$):

$$\hat{H} = -2J_2(\hat{S}_{Cu2}\hat{S}_{rad2} + \hat{S}_{Cu2}\hat{S}_{rad3}) - 2J_1(\hat{S}_{Gd1}\hat{S}_{rad1} + \hat{S}_{Gd1}\hat{S}_{rad2} + \hat{S}_{Gd2}\hat{S}_{rad3} + \hat{S}_{Gd2}\hat{S}_{rad4}) \\ -2J_3(\hat{S}_{rad1}\hat{S}_{rad2} + \hat{S}_{rad3}\hat{S}_{rad4}) \quad (1)$$

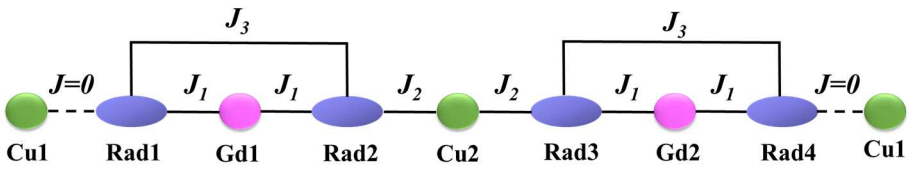

Scheme 2. Magnetic communications in complex **1**.

The best fit parameters are J_1 = 3.47 cm^{-1}, J_2 = 12.09 cm^{-1}, J_3 = –4.15 cm^{-1}, g_{Cu}= 2.15, g_{Gd} = 2.00, and g_{rad} = 2.00 (fixed). The ferromagnetic Gd^{III}-NO interaction, J_1, is an expectable outcome due to the large Gd-O-N-C torsion angles of 75.30(9)° and 63.42(8)°, which favor the electron transfer from the π* orbital of the radical to the 5d/6s empty orbitals of the Gd^{III}.[17] The ferromagnetic Cu^{II}-NO interaction (J_2) is related to the axial coordination of the NO units to Cu^{II} ion which leads to the orthogonality of magnetic orbitals ($d_{x^2-y^2}$ for Cu^{II} ion and π* for radical). The parameter J_3 should be considered as an evaluation of two contributions that balance each other; one is the next-neighbor antiferromagnetic interaction between the two NO groups via the Gd^{III},[18] the other is the ferromagnetic NIT-NIT interaction through the benzene.[19] The negative J_3 suggests that the former is stronger, which was observed for other Gd- biradical compounds.[15, 20], but this antiferromagnetic interaction between next-neighbors is largely compensated by the intra-ligand ferromagnetic NIT-NIT interaction.

For complex **2**, the $\chi_M T$ value obtained at 300K is 30.36 cm^3 K mol^{-1} (Figure 3), in good agreement with the 30.96 cm^3 K mol^{-1} expected for two Dy^{III} ions ($^6H_{15/2}$, g = 4/3, C = 14.17 cm^3 K mol^{-1}), three Cu^{III} ions (S = 1/2, g = 2, C = 0.375 cm^3 K mol^{-1}) and four radicals (S = 1/2, g = 2, C = 0.375 cm^3 K mol^{-1}) in the absence of exchange interactions. The variation of $\chi_M T$ with temperature is similar to that of the Gd derivative, thus supporting ferromagnetic Cu^{II}/ Dy^{III}-nitroxide interactions. The field dependence of the magnetization at 2 K (Figure 3) also shows a fast increase at low fields followed by a smoother augmentation above 10 kOe to reach 19.11 Nβ at 70 kOe.

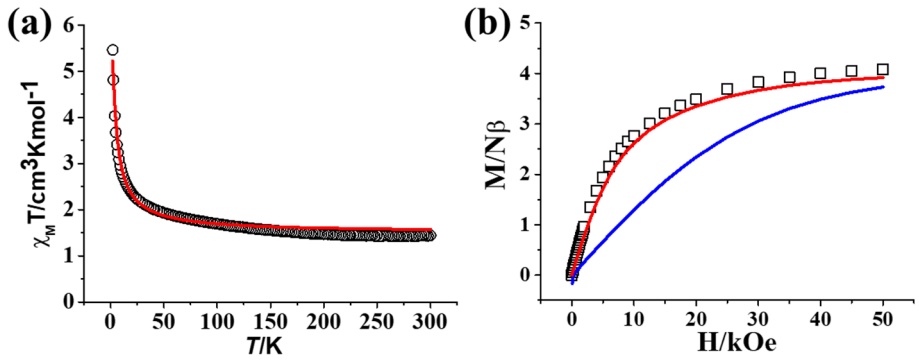

Figure 4. (a) Plot of $\chi_M T$ versus T for **3**. (b) Field-dependent magnetization for **3** (2.0K). The red line is the best fit and the blue line shows the theoretical behavior calculated by the Brillouin function for four S = $^1/_2$ independent spins.

For [$LnCu_2$(hfac)$_7$(NITPhMeImbis)] chain compounds **3**-**5**, the $\chi_M T$ values obtained at 300 K are 1.45 cm^3 K mol^{-1} for **3,** 16.45 cm^3 K mol^{-1} for **4,** and 13.62 cm^3 K mol^{-1} for **5** (Figures 4a and 5), in good agreement with the anticipated values for each spin system (1.50 cm^3 K mol^{-1} for **3,** 15.67 cm^3 K mol^{-1} for **4,** and 13.32 cm^3 K $mol^{-1}$for **5**, considering one Ln^{III} ion (Y^{III}: diamagnetic, Dy^{III}: $^6H_{15/2}$, g = 4/3, C = 14.17 cm^3 K mol^{-1}, Tb^{III}: $^7F_6$, g = 3/2, C = 11.82 cm^3 K mol^{-1}), two Cu^{II} ions (S = 1/2, g = 2, C = 0.375 cm^3 K mol^{-1}) and two radicals (S = 1/2, g = 2, C = 0.375 cm^3 K mol^{-1}) without exchange interactions). For all the derivatives the $\chi_M T$ values gradually increase with decreasing temperature and reach large values (5.46 cm^3 K mol^{-1} for **3** at 2 K, 74.8 cm^3 K mol^{-1} for **4** at 3 K, 71.49 cm^3 K mol^{-1} for **5** at 3 K), which eventually drop for **4** and **5** reaching respectively 64.41 cm^3 K mol^{-1} and 55.81 cm^3 K mol^{-1} at 2 K. Such behavior is characteristic for exchange interactions developing along the 1D spin systems. The field dependence of the magnetization for **3** shows a steady increase with field to reach 4 $N\beta$ for 50 kOe at 2 K (Figure 4b), in agreement with

the theoretical saturation value of 4 $N\beta$ anticipated in case of a paramagnetic system or ferromagnetic Cu-Rad and Rad-Rad interactions. The magnetization calculated by the Brillouin function for four independent $S = {}^1/_2$ spin centers runs clearly below the experimental behavior (blue trace in Figure 4b), supporting the existence of ferromagnetic interaction for the Cu^{II}-NO groups and possibly for the biradical moieties in the system. The M versus H behaviors for **4** and **5** at 2.0 K exhibit a very rapid increase in low fields followed by a much smoother evolution to reach 9.26 $N\beta$ at 50 kOe for **4** and 8.44 $N\beta$ at 70 kOe for **5** (Figures S12 and S13).

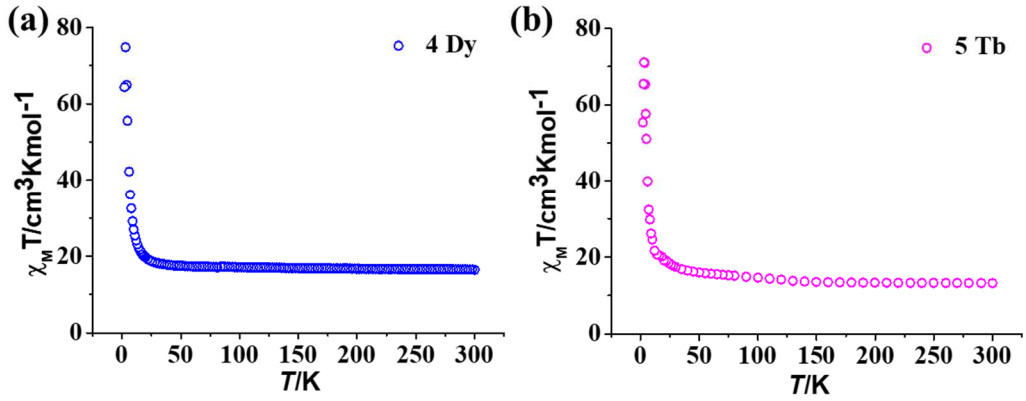

Figure 5. Plots of $\chi_M T$ versus T for **4** (a) and **5** (b).

For Ising-like or anisotropic Heisenberg spin-chains the magnetic susceptibility follows an exponential dependence with the temperature according $\chi_M T = C_{eff} \exp[\Delta\xi/(k_B T)]$, where $\Delta\xi$ stands for the energy to create a domain wall in the chain, k_B is Boltzmann constant, and C_{eff} the effective Curie constant.[21] The plots of $\ln(\chi_M T)$ versus 1/T for **4** and **5** (Figures S14 and S15) show indeed a linear variation in the temperature range 4.6-19 K and 7-22 K, respectively. The analysis of these linear parts gave $\Delta\xi/k_B = 6.4$ K and $C_{eff} = 14.2$ cm^3 mol^{-1} K for **4**, $\Delta\xi/k_B = 9.7$ K and $C_{eff} = 12.27$ cm^3 mol^{-1} K for **5**, hence confirming that both of **4** and **5** behave as Ising-like chains.

The magnetic interactions taking place in **3** have been assessed by using a closed loop model with three [Cu-NIT-Y-NIT] units plus three uncoupling Cu^{II} ions (Scheme 3). In this model, the active exchange pathways are J_1, the interaction between Cu^{II} ion and the coordinated nitroxide radicals and J_2. We recall that J_2 accounts for the apparent interaction within the biradical moiety that comprises the next-neighbor interactions between the two NIT groups mediated by the 5s/4d orbitals of Y^{III} ion and the interaction between the two NIT units through the benzene ring. The modeling

performed with PHI program[16] is derived from the Hamiltonian (equation 2) given below plus three independent Cu centers (S = ½):

$$\hat{H} = -2J_1(\hat{S}_{Cu1}\cdot\hat{S}_{Rad1} + \hat{S}_{Cu1}\cdot\hat{S}_{Rad6} + \hat{S}_{Cu2}\cdot\hat{S}_{Rad2} + \hat{S}_{Cu2}\cdot\hat{S}_{Rad3} + \hat{S}_{Cu3}\cdot\hat{S}_{Rad4} + \hat{S}_{Cu3}\cdot\hat{S}_{Rad5}) - 2J_2(\hat{S}_{Rad1}\cdot\hat{S}_{Rad2} + \hat{S}_{Rad3}\cdot\hat{S}_{Rad4} + \hat{S}_{Rad5}\cdot\hat{S}_{Rad6}) \quad (2)$$

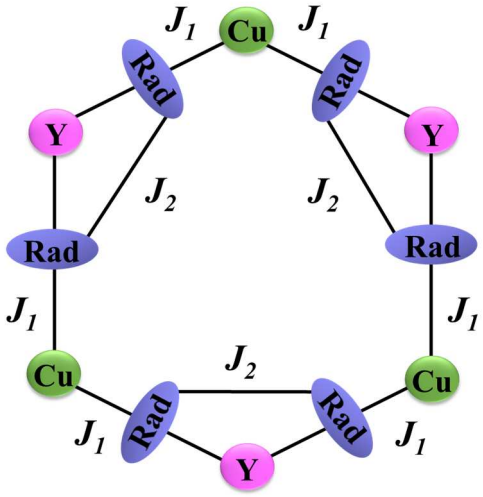

Scheme 3. Magnetic exchange pathway in complex **3**.

The simultaneous analyses of the $\chi_M T$ and magnetization data yielded: J_1 = 14.01 cm^{-1}, J_2 = 7.13 cm^{-1}, g_{Cu} = 2.01, g_{rad} = 2.00 (fixed). The positive J_1 value confirms the anticipated ferromagnetic Cu^{II}-NO interaction also found in **1**. The positive J_2 reveals that the exchange interaction between radicals via the benzene ring is stronger and imposes an overall ferromagnetic interaction. This is not surprising because it has been shown that Y^{III} is less efficient in mediation the rad-rad interaction.[18b]

Dynamic susceptibility studies

AC magnetic susceptibility measurements have been used to explore the spin dynamics in complexes **2**, **4** and **5**. For **2,** the data recorded in the absence of a static field showed a frequency dependent out of phase susceptibility signal, χ'', indicative of slow relaxation behavior (Figure S16) but no peaks was found above 2 K for an AC frequency range of 100-800 Hz, which may be due to the quantum tunneling of the magnetization (QTM). The application of a static magnetic field of 3000 Oe shifted the data set to higher temperatures and the χ'' versus T behaviors obtained for high frequencies exhibited a well-defined maximum (Figure S17). The extracted relaxation times, τ, were

analyzed with an Arrhenius law, $\tau = \tau_0 \exp(U_{eff}/k_B T)$ (Figure S18), resulting in an energy barrier U_{eff}/k_B = 13 K and pre-exponential factor $\tau_0 = 5.8 \times 10^{-8}$ s.

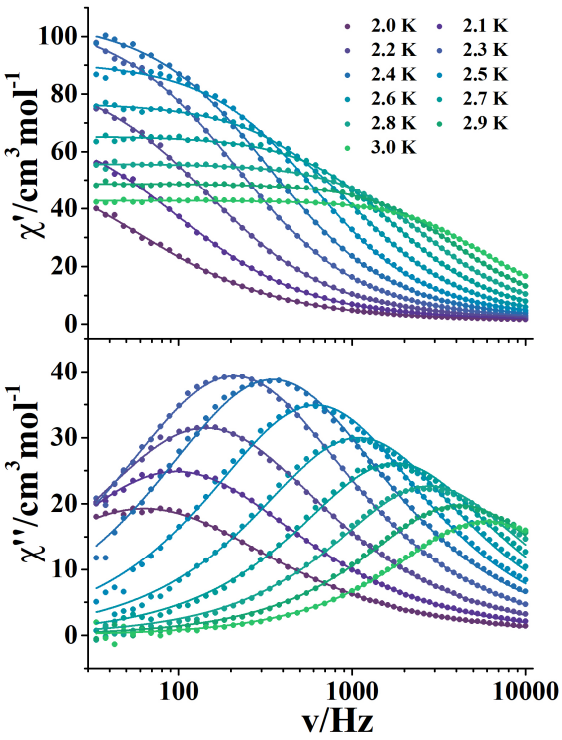

Figure 6. Frequency-dependent ac signals under a zero dc field for compound **4** (solid lines: the fits to the Debye model).

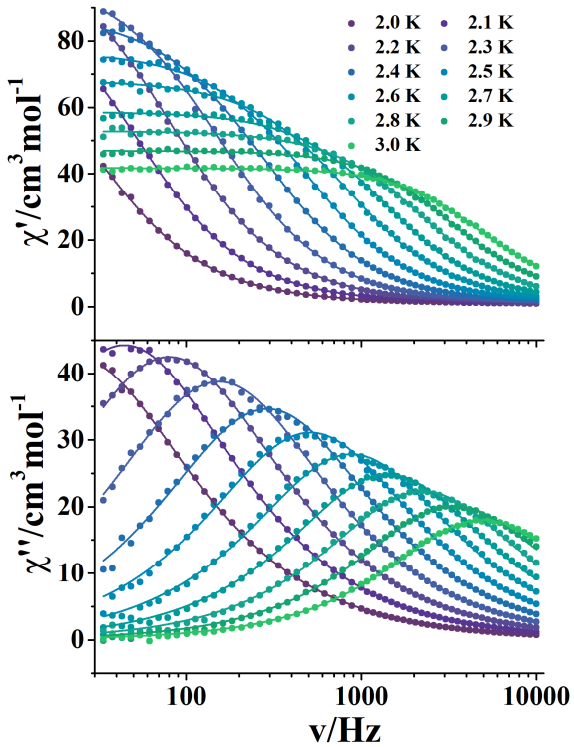

Figure 7. Frequency-dependent ac signals under a zero dc field for compound **5** (solid lines: the fits to the Debye model).

The AC susceptibility behaviors for **4** and **5** recorded in the absence of a static field are indicative for a slow relaxation of the magnetization below 5 K (Figures 6, 7, S19 and S20). The Cole-Cole diagrams (Figures 8b and 9b) are semicircular in the temperature range 2.0-3.0 K. The distribution width of the relaxation times, evaluated by the parameter α in the generalized Debye model,[22] gave values of α in the range of 0.06-0.34 for **4** and 0.07-0.17 for **5**, which are indicative of moderate distribution of the relaxation time for **4** while narrow distribution for **5**. The $\ln\tau$ *vs.* $(1/T)$ plots exhibit the linear dependence (Figures 8a and 9a). The analysis of these behaviors by the Arrhenius equation, $\tau = \tau_0 \exp(\Delta_\tau / k_B T)$, gave activation energies for spin flipping of $\Delta_\tau/k_B = 28.34$ K for **4** with $\tau_0 = 2.5 \times 10^{-9}$ s, and $\Delta_\tau/k_B = 32.80$ K with $\tau_0 = 6.1 \times 10^{-10}$ s for **5**.

For Ising-like spin chains, the energy barrier consists of the contributions arising from the correlation energy (Δ_ξ) and the blocking energy (Δ_A) resulting from the magnetic anisotropic of the repeating units. Assuming that the relaxation behaviors of **4** and **5** occur in a finite size regime, the anisotropic energy barriers is given by $\Delta_A = \Delta_\tau - \Delta_\xi$.[3d, 23] Hence, Δ_A can be estimated to be about 22 K and 23 K for **4** and **5**, respectively.

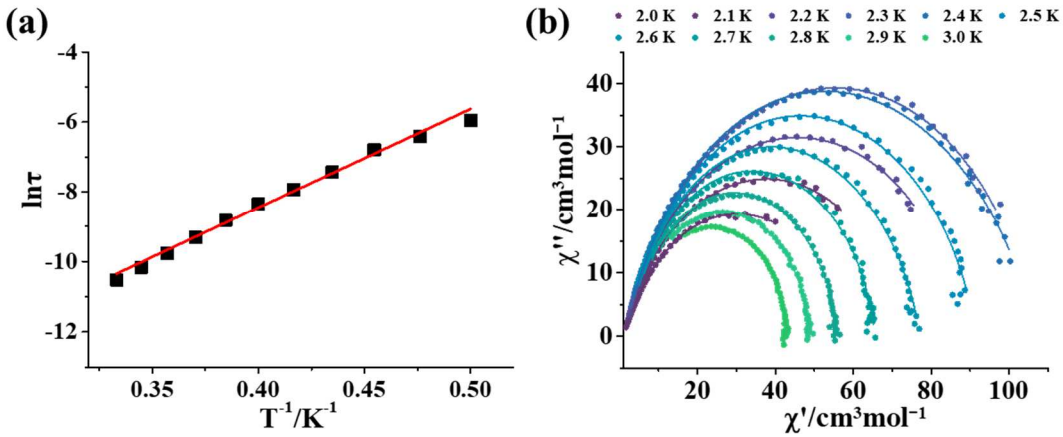

Figure 8. (a) The $\ln\tau$ vs. $1/T$ plot for **4** (red-line: fitting results by the Arrhenius law). (b) Cole-Cole curves for **4** in 0 Oe (the solid lines: the fits to the Debye model).

From these investigations, it appears that complex **2** could be considered as a field induced SMM whereas the chain compound **4** and **5** are SCMs. Remarkably, the same SCM characteristics are achieved for the Tb and Dy chains, an observation already made for related biradical-Cu-Ln SCMs.[13]

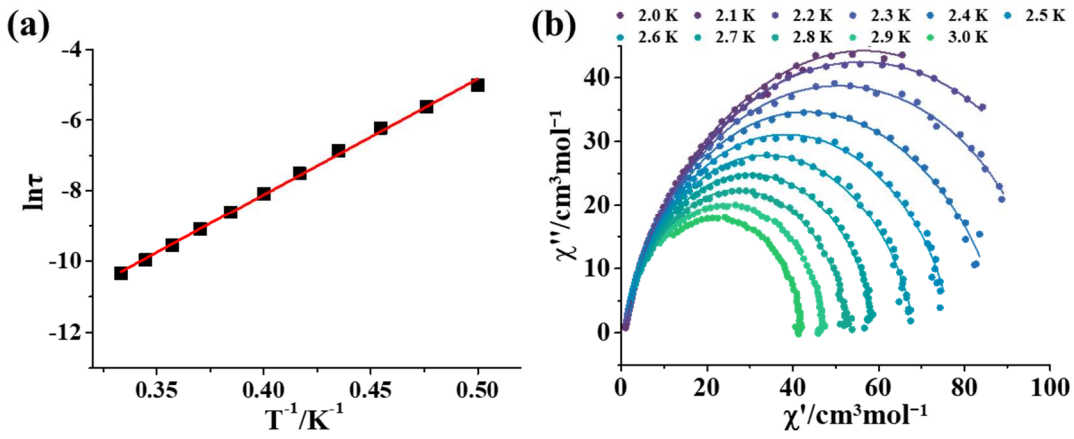

Figure 9. (a) The lnτ vs. 1/*T* plot for **5** (red-line: fitting results by the Arrhenius law). (b) Cole-Cole curves for **5** in 0 Oe (the solid lines: the fits to the Debye model).

It is interesting to note the distinct magnetic relaxation behaviors observed for the two Dy derivatives **2** and **4**, a much higher energy barrier being achieved by 1D-[$DyCu_2(hfac)_7$(NITPhMeImbis)]. In light of crystal structures, complex **2** can be regarded as a fragment of the chain **4**. The enhanced energy barrier moving from discrete to the 1D compound is a nice illustration of the contribution of the correlation energy, Δ_ξ, expected for Ising-type spin chains. In **4**, it results from the propagation along the chain of the ferromagnetic Cu-NO and Dy-NO exchange interactions. In this process, the reduction of the detrimental antiferromagnetic next-neighbor contribution by the ferromagnetic biradical ligand achieves quite high energy barriers compared to other 2*p*-3*d*-4*f* chain compounds.

Conclusion

In summary, a new nitronyl nitroxide biradical with 2-methylimidazole group allows to obtain either discrete or 1D 2*p*-3*d*-4*f* complexes. Interestingly, the chain can be considered as resulting from the assemblage of the nona-spin complexes. This allows us to highlight the contribution of the 1D exchange correlation on magnetic relaxation characteristics of these compounds.

This study confirms the essential contribution of a ferromagnetic biradicals moiety in the magnetic features, especially the magnetization blocking, of compounds based on NIT-Ln-NIT units. The combination of paramagnetic 3d and 4f ions with a biradical ligand is clearly a successful strategy to construct SCMs.

Experimental Section

Materials and characterizations

CH_2Cl_2, *n*-heptane, and all other initial chemicals were purchased from commercial sources in AR grade and used without further purification. The nitronyl nitroxide biradical NITPhMeImbis was synthesized with reference to the reported literature.[24] The elemental analysis (C, H, and N) was performed on a Perkin–Elmer 240 elemental analyzer. Infrared spectra (4000–400 cm^{-1}) were collected on a Bruker Tensor 27 spectrophotometer with KBr pellets. The powder X-ray diffraction (PXRD) data for **1–4** were obtained using a Rigaku Ultima IV diffractometer with Cu/Kα radiation at room temperature. Magnetic measurements were performed on Quantum Design SQUID- MPMS 5S, VSM and PPMS-9 magnetometers. The crystalline powder samples containing Dy and Tb ions were mixed with grease or liquid eicosane to avoid orientation effects. Direct current (dc) magnetic susceptibility data were corrected in the light of Pascal's constants.[25]

Syntheses

Synthesis of $[Ln_2Cu_3(hfac)_{12}(NITPhMeImbis)_2]$ (Ln = Gd, 1; Dy, 2)

0.01 mmol of $Ln(hfac)_3{\cdot}2H_2O$ ($Gd(hfac)_3{\cdot}2H_2O$: 0.0082 g; $Dy(hfac)_3{\cdot}2H_2O$: 0.0082 g) and 0.02 mmol (0.0096 g) of $Cu(hfac)_2$ were dissolved in 15 ml of boiling *n*-C_7H_{16}, and kept at reflux for 4 h. Then the obtained solution was cooled to 80℃ and 0.01 mmol (0.0047 g) of NITPhMeImbis dissolved in 8 ml of CH_2Cl_2 was added, the reaction was maintained at 80℃ for half an hour. The resulted solution was cooled to room temperature and then filtered. The filtrate was left at room temperature to slowly concentrate, and after two weeks, gray-blue plate crystals were isolated.

$[Gd_2Cu_3(hfac)_{12}(NITPhMeImbis)_2]$ (1)

Yield 36%; $C_{108}H_{76}Cu_3F_{72}N_{12}O_{32}Gd_2$ (3926.92 g mol^{-1}); Elem. Anal. (%.) found (calcd): C, 33.03 (32.92); N, 4.28 (4.21); H, 1.95 (1.84). FT-IR (cm^{-1}): 1648 (s), 1500 (m), 1357 (m), 1251 (s), 1205 (s), 1135 (s), 798 (s), 740 (m), 659 (s), 584 (s), 544 (m).

$[Dy_2Cu_3(hfac)_{12}(NITPhMeImbis)_2]$ (2)

Yield 33%; $C_{108}H_{76}Cu_3F_{72}N_{12}O_{32}Dy_2$ (3937.42 g mol^{-1})**;** Elem. Anal. (%) found (calcd): C, 32.94 (32.81); N, 4.27 (4.24); H, 1.95 (1.83). FT-IR (cm^{-1}): 1648 (s), 1501 (m), 1359 (m), 1252 (s), 1206 (s), 1137 (s), 798 (s), 741 (m), 659 (s), 584 (s), 544 (m).

Preparation of $[LnCu_2(hfac)_7(NITPhMeImbis)]$ (Ln = Y, 3; Dy, 4; Tb, 5)

$Ln(hfac)_3{\cdot}2H_2O$ (0.01 mmol, $Y(hfac)_3{\cdot}2H_2O$: 0.0075 g; $Dy(hfac)_3{\cdot}2H_2O$: 0.0082 g $Tb(hfac)_3{\cdot}2H_2O$: 0.0082 g) and $Cu(hfac)_2$ (0.02 mmol, 0.0096 g) were dissolved in boiling *n*-heptane (15mL), and then the obtained solution was kept under reflux for 4 h. A solution of NITPhMeImbis (0.01 mmol, 0.0047 g) in dry CH_2Cl_2 (8 mL) was then added slowly to the solution, and the reflux maintained for 30 minutes. Afterwards, the solution was cooled to room temperature and filtered. Subsequently, the filtrate was left undisturbed to evaporate, yielding deep blue block crystals about five days later.

$[YCu_2(hfac)_7(NITPhMeImbis)]$ (**3**)

Yield 56%; $C_{59}H_{39}Cu_2F_{42}YN_6O_{18}$ (2133.95 g mol^{-1}); Elem. Anal. (%) found (calcd): C, 33.32 (33.21); N, 4.06 (3.94); H, 1.96 (1.84). FT-IR (cm^{-1}): 1650 (s), 1509 (m), 1355 (m), 1253 (s), 1199 (s), 1136 (s), 798 (s), 740 (m), 658 (s), 585 (s), 535 (m).

$[DyCu_2(hfac)_7(NITPhMeImbis)]$ (**4**)

Yield 59%; $C_{59}H_{39}Cu_2F_{42}DyN_6O_{18}$ (2207.54 g mol^{-1}); Elem. Anal. (%) found (calcd): C, 32.04 (32.10); N, 3.70 (3.81); H, 1.86 (1.78). FT-IR (cm^{-1}): 1650 (s), 1509 (m), 1355 (m), 1255 (s), 1201 (s), 1137 (s), 799 (s), 741 (m), 658 (s),585 (s), 537 (m).

$[TbCu_2(hfac)_7(NITPhMeImbis)]$ (**5**)

Yield 54%; $C_{59}H_{39}Cu_2F_{42}TbN_6O_{18}$ (2203.96 g mol^{-1}); Elem. Anal. (%) found (calcd): C, 32.24 (32.15); N, 3.86 (3.81); H, 1.89 (1.78). FT-IR (cm^{-1}): 1649 (s), 1510 (m), 1354 (m), 1254 (s), 1200 (s), 1136 (s), 798 (s), 742 (m), 658 (s), 586 (s), 536 (m).

Crystallography

X-ray crystallographic data for all complexes were acquired on a Rigaku Saturn diffractometer equipped with a CCD detector and graphite-monochromatic Mo-Kα radiation (λ = 0.71073 Å) at 113 K. The absorption corrections were performed by the multi-scan technique. By the use of SHELXS-2014 and SHELXL-2014 software packages, the structures were solved by the direct methods and refined by full–matrix least–squares on F^2.[26] All non-H atoms were refined anisotropically, while all H atoms of organic ligands were placed in calculated positions and refined isotropically. Eventually, the disordered atoms were properly corrected and rationalized by adopting DELU, ISOR, RIGU and SIMU restraints. The final crystallographic data and refinement details of the five compounds are listed in Table S1. The important bond lengths and angles are shown in Tables S2 and S4–S8.

Deposition Number(s) <url href = "https://www.ccdc.cam.ac.uk/services/structures?id = doi:10.1002/chem.202203852"> 2222149 (for **1**), 2222148 (for **2**), 2222152 (for **3**), 2222150 (for **4**), 2222151 (for **5**)</url> contain(s) the supplementary crystallographic data for this paper. These data are provided free of charge by the joint Cambridge Crystallographic Data Centre and Fachinformationszentrum Karlsruhe <url href=" http://www.ccdc.cam.ac.uk/structures ">Access Structures service</url>.

Acknowledgements

This work was financially supported by the National Key R&D Program of China (2018YFA0306002) and the National Natural Science Foundation of China (No. 21773122). The authors thank Mr. Jean-François Meunier (LCC) for his technical assistance in collecting the magnetic data.

Conflict of Interest

There are no conflicts to declare.

References

[1] a) L. Bogani, A. Vindigni, R. Sessoli, D. Gatteschi, *J. Mater. Chem.* **2008**, *18*, 4750-4758; b) D. N. Woodruff, R. E. P. Winpenny, R. A. Layfield, *Chem. Rev.* **2013**, *113*, 5110-5148; c) S. Demir, I.-R. Jeon, J. R. Long, T. D. Harris, *Coord. Chem. Rev.* **2015**, *289-290*, 149-176; d) M. G. F. Vaz, M. Andruh, *Coord. Chem. Rev.* **2021**, *427*, 213611.

[2] a) K. Bernot, F. Pointillart, P. Rosa, M. Etienne, R. Sessoli, D. Gatteschi, *Chem. Commun.* **2010**, *46*, 6458-6460; b) J. Wang, J.-N. Li, S.-L. Zhang, X.-H. Zhao, D. Shao, X.-Y. Wang, *Chem. Commun.* **2016**, *52*, 5033-5036; c) S. Kanegawa, S. Karasawa, M. Maeyama, M. Nakano, N. Koga, *J. Am. Chem. Soc.* **2008**, *130*, 3079-3094; d) J. D. Rinehart, M. Fang, W. J. Evans, J. R. Long, *J. Am. Chem. Soc.* **2011**, *133*, 14236-14239; e) K. Wang, D. Qi, H. Wang, W. Cao, W. Li, T. Liu, C. Duan, J. Jiang, *Chem. Eur. J.* **2013**, *19*, 11162-11166; f) X.-L. Wang, L.-C. Li, D.-Z. Liao, *Inorg. Chem.* **2010**, *49*, 4735-4737; g) F.-S. Guo, R. A. Layfield, *Chem. Commun.* **2017**, *53*, 3130-3133; h) N. Mavragani, D. Errulat, D. A. Gálico, A. A. Kitos, A. Mansikkamäki, M. Murugesu, *Angew. Chem., Int. Ed.* **2021**, *60*, 24206-24213.

[3] a) A. Caneschi, D. Gatteschi, N. Lalioti, C. Sangregorio, R. Sessoli, G. Venturi, A. Vindigni, A. Rettori, M. G. Pini, M. A. Novak, *Angew. Chem., Int. Ed.* **2001**, *40*, 1760-1763; b) N. Ishii, Y. Okamura, S. Chiba, T. Nogami, T. Ishida, *J. Am. Chem. Soc.* **2008**, *130*, 24-25; c) M. G. F. Vaz, R. A. A. Cassaro, H. Akpinar, J. A. Schlueter, P. M. Lahti, M. A. Novak, *Chem. Eur. J.* **2014**, *20*, 5460-5467; d) K. Bernot, L. Bogani, A. Caneschi, D. Gatteschi, R. Sessoli, *J. Am. Chem. Soc.* **2006**, *128*, 7947-7956; e) T. Han, W. Shi, Z. Niu, B. Na, P. Cheng, *Chem. Eur. J.* **2013**, *19*, 994-1001; f) P. Hu, X. Wang, Y. Ma, Q. Wang, L. Li, D. Liao, *Dalton Trans.* **2014**, *43*, 2234-2243.

[4] a) M. N. Leuenberger, D. Loss, *Nature* **2001**, *410*, 789-793; b) M. Affronte, *J. Mater. Chem.* **2009**, *19*, 1731-1737; c) P. C. E. Stamp, A. Gaita-Ariño, *J. Mater. Chem.* **2009**, *19*, 1718-1730; d) S. Sanvito, *Chem. Soc. Rev.* **2011**, *40*, 3336-3355; e) G. A. Timco, T. B. Faust, F. Tuna, R. E. P. Winpenny, *Chem. Soc. Rev.* **2011**, *40*, 3067-3075.

[5] S. Demir, M. I. Gonzalez, L. E. Darago, W. J. Evans, J. R. Long, *Nat. Commun.* **2017**, *8*, 2144.

[6] F. Liu, L. Spree, D. S. Krylov, G. Velkos, S. M. Avdoshenko, A. A. Popov, *Acc. Chem. Res.* **2019**, *52*, 2981-2993.

[7] F. Liu, G. Velkos, D. S. Krylov, L. Spree, M. Zalibera, R. Ray, N. A. Samoylova, C.-H. Chen, M. Rosenkranz, S. Schiemenz, F. Ziegs, K. Nenkov, A. Kostanyan, T. Greber, A. U. B. Wolter, M. Richter, B. Büchner, S. M. Avdoshenko, A. A. Popov, *Nat. Commun.* **2019**, *10*, 571.

[8] X. Liu, X. Feng, K. R. Meihaus, X. Meng, Y. Zhang, L. Li, J. L. Liu, K. S. Pedersen, L. Keller, W. Shi, Y. Q. Zhang, P. Cheng, J. R. Long, *Angew. Chem., Int. Ed.* **2020**, *59*, 10610-10618.

[9] a) C. Coulon, R. Clérac, L. Lecren, W. Wernsdorfer, H. Miyasaka, *Phys. Rev. B* **2004**, *69*, 132408; b) W.-X. Zhang, R. Ishikawa, B. Breedlove, M. Yamashita, *RSC Adv.* **2013**, *3*, 3772-3798.

[10] F. Houard, Q. Evrard, G. Calvez, Y. Suffren, C. Daiguebonne, O. Guillou, F. Gendron, B. Le Guennic, T. Guizouarn, V. Dorcet, M. Mannini, K. Bernot, *Angew. Chem., Int. Ed.* **2020**, *59*, 780-784.

[11] M. Zhu, L. Li, J.-P. Sutter, *Inorg. Chem. Front.* **2016**, *3*, 994-1003.

[12] a) M. Zhu, P. Hu, Y. Li, X. Wang, L. Li, D. Liao, V. M. L. Durga Prasad Goli, S. Ramasesha, J.-P. Sutter, *Chem. Eur. J.* **2014**, *20*, 13356-13365; b) M. Zhu, X. Mei, Y. Ma, L. Li, D. Liao, J.-P. Sutter, *Chem. Commun.* **2014**, *50*, 1906-1908; c) X. Huang, K. Wang, J. Han, J. Xie, L. Li, J. P. Sutter, *Dalton Trans.* **2021**, *50*, 11992-11998.

[13] a) J. Xie, H. D. Li, M. Yang, J. Sun, L. C. Li, J. P. Sutter, *Chem. Commun.* **2019**, *55*, 3398-3401; b) J. Sun, J. Xie, L. Li, J.-P. Sutter, *Inorg. Chem. Front.* **2020**, *7*, 1949-1956.

[14] M. Llunell, D. Casanova, J. Cirera, P. Alemany, S. Alvarez, *SHAPE 2.1*, University of Barcelona, Barcelona, **2013**.

[15] H. Li, J. Sun, M. Yang, Z. Sun, J. Tang, Y. Ma, L. Li, *Inorg. Chem.* **2018**, *57*, 9757-9765.

[16] N. F. Chilton, R. P. Anderson, L. D. Turner, A. Soncini, K. S. Murray, *J. Comput. Chem.* **2013**, *34*, 1164-1175.

[17] T. Gupta, T. Rajeshkumar, G. Rajaraman, *Phys. Chem. Chem. Phys.* **2014**, *16*, 14568-14577.

[18] a) C. Benelli, A. Caneschi, D. Gatteschi, L. Pardi, P. Rey, *Inorg. Chem.* **1990**, *29*, 4223-4228; b) J.-P. Sutter, M. L. Kahn, S. Golhen, L. Ouahab, O. Kahn, *Chem. Eur. J.* **1998**, *4*, 571-576.

[19] L. Catala, J. Le Moigne, N. Kyritsakas, P. Rey, J. J. Novoa, P. Turek, *Chem. Eur. J.* **2001**, *7*, 2466-2480.

[20] L. Tian, Y.-Q. Sun, B. Na, P. Cheng, *Eur. J. Inorg. Chem.* **2013**, *2013*, 4329-4335.

[21] C. Coulon, H. Miyasaka, R. Clérac, *Struct. Bonding (Berlin)* **2006**, *122*, 163.

[22] a) C. Dekker, A. F. M. Arts, H. W. de Wijn, A. J. van Duyneveldt, J. A. Mydosh, *Phys. Rev. B* **1989**, *40*, 11243-11251; b) S. M. J. Aubin, Z. Sun, L. Pardi, J. Krzystek, K. Folting, L.-C. Brunel, A. L. Rheingold, G. Christou, D. N. Hendrickson, *Inorg. Chem.* **1999**, *38*, 5329-5340.

[23] R. J. Glauber, *J. Math. Phys.* **1963**, *4*, 294-307.

[24] a) E. F. Ullman, L. Call, J. H. Osiecki, *J. Org. Chem.* **1970**, *35*, 3623-3631; b) E. F. Ullman, J. H. Osiecki, D. G. B. Boocock, R. Darcy, *J. Am. Chem. Soc.* **1972**, *94*, 7049-7059.

[25] T. A. Stephenson, E. A. Boudreaux, L. N. Mulay, *Theory and Applications of Molecular Paramagnetism, Vol. 92*, **1977**.

[26] a) G. M. Sheldrick, *SHELXS-2014, Program for structure solution*, Universität of Göttingen, Göttingen, Germany, **2014**.; b) G. M. Sheldrick, *SHELXL-2014, Program for structure refinement*, Universität of Göttingen, Göttingen, Germany, **2014**.

SUPPORTING INFORMATION

Contents

Table S1. Crystallographic data for **1**–**5**.

Complex	**1 Gd**	**2 Dy**	**3 Y**	**4 Dy**	**5 Tb**
Formula	$C_{108}H_{76}Cu_3F_{72}N_{12}O_{32}Ln_2$		$C_{59}H_{39}Cu_2F_{42}N_6O_{18}Ln$		
M(g·mol^{-1})	3926.92	3937.42	2133.95	2207.54	2203.96
T(K)	113(2)	113(2)	113(2)	113(2)	113(2)
Crystal system	triclinic	triclinic	triclinic	triclinic	triclinic
Space group	$P\bar{1}$	$P\bar{1}$	$P\bar{1}$	$P\bar{1}$	$P\bar{1}$
a(Å)	11.9037(6)	11.8503(6)	13.2210(6)	13.2050(8)	13.1841(5)
b(Å)	17.0977(7)	16.9919(9)	16.3885(10)	16.3620(10)	16.3945(9)
c(Å)	18.0145(8)	17.9846(9)	19.7726(9)	19.7934(12)	19.7714(8)
α(deg)	92.691(3)	92.670(4)	91.353(4)	91.287(5)	91.394(4)
β(deg)	96.480(4)	96.455(4)	90.198(4)	90.225(5)	90.126(3)
γ(deg)	94.199(4)	94.080(4)	110.779(5)	110.640(6)	110.785(4)
V(Å$^{3)}$	3627.6(3)	3583.8(3)	4004.1(4)	4000.7(4)	3993.9(3)
Z	1	1	2	2	2
D_{calcd}(g·cm^{-3})	1.798	1.824	1.770	1.833	1.833
M(mm^{-1})	1.500	1.635	1.410	1.616	1.569
θ(deg)	2.177-25.350	1.703-25.350	1.660-24.713	1.66-24.71	1.660-24.712
F(000)	1927	1931	2108	2162	2160
Reflns collected	36130	35819	37097	37519	37440
Unique reflns/R_{int}	13296/ 0.0903	13126/0.0903	13645/0.0742	13637/0.1249	13598/0.0583
GOF(F^2)	1.023	1.015	1.026	1.025	1.121
R_1/wR_2(I>2σ(I))	0.0630/0.1495	0.0612/0.1251	0.0853/0.2198	0.0849/0.2098	0.0663/0.1866
R_1/wR_2(all data)	0.0913/0.1698	0.1045/0.1521	0.1474/0.2659	0.1392/0.2481	0.0876/0.2048

$R_1 = \Sigma(||Fo| - |Fc||)/\Sigma|Fo|$, $wR_2 = [\Sigma w(|Fo|^2 - |Fc|^2)^2/\Sigma w(|Fo|^2)^2]^{1/2}$

Table S2. Key bond lengths/angles [Å/°] for **1**–**5**

Complex	**1 Gd**	**2 Dy**	**3 Y**	**4 Dy**	**5 Tb**
Ln-O_{rad}	2.356(4), 2.465(4)	2.328(4), 2.453(4)	2.377(5), 2.359(5)	2.386(6), 2.348(7)	2.394(5), 2.369(5)
Ln-O_{hfac}	2.331(5)-2.4001(5)	2.301(5)-2.368(5)	2.288(5)-2.370(6)	2.298(7)-2.361(7)	2.303(5)-2.372(5)
O_{rad}-Ln-O_{rad}	83.90(2)	84.19(2)	81.40(2)	82.22(2)	81.61(2)
N-O-Ln	139.2(4), 141.9(4)	138.9(4), 142.2(4)	140.2(4), 143.3(5)	141.3(5), 144.3(6)	140.1(4), 142.6(5)
Cu-O_{hfac}	1.931(4)-2.214(4)	1.928(4)-2.206(4)	1.903(7)-2.193(7)	1.919(9)-2.187(9)	1.911(5)-2.182(6)
Cu-N	1.971(5)	1.962(5)	1.988(7)	1.985(8)	1.976(6)
Cu-O_{rad}	2.525(4)	2.512(4)	2.457(7), 2.526(6)	2.453(9), 2.526(8)	2.455(7), 2.508(6)
O-Cu-N	93.7(2)	93.2(2)	99.1(3)	98.6(3)	98.9(3)

Table S3. Continuous Shape Measures (CShM) calculation for **1-5**

Complex	**BTPR-8**	JBTPR-8	SAPR-8	TDD-8
1 Gd	**0.968**	1.751	2.445	1.803
2 Dy	**0.936**	1.706	2.396	1.829
3 Y	**1.021**	1.898	3.188	1.700
4 Dy	**1.098**	1.958	3.309	1.733
5 Tb	**1.034**	1.914	3.247	1.739

BTPR-8: C_{2v}, Biaugmented trigonal prism; JBTPR-8: C_{2v}, Biaugmented trigonal prism J50; SAPR-8: D_{4d}, Square antiprism; TDD-8: D_{2d}, Triangular dodecahedron

Table S4. Selected bond lengths [Å] and angles [°] for **1**

Bond distances			
Gd(1)-O(2)	2.356(4)	Cu(2)-O(11)#1	1.934(4)
Gd(1)-O(7)	2.353(5)	Cu(2)-O(11)	1.934(4)
Gd(1)-O(1)	2.465(4)	Cu(2)-O(10)	1.938(4)
Gd(1)-O(6)	2.331(5)	Cu(2)-O(10)#1	1.938(4)
Gd(1)-O(8)	2.389(5)	Cu(1)-O(12)	1.958(4)
Gd(1)-O(4)	2.401(5)	Cu(1)-O(14)	1.931(4)
Gd(1)-O(3)	2.345(5)	Cu(1)-O(15)	1.947(5)
Gd(1)-O(5)	2.379(5)	Cu(1)-O(13)	2.214(4)
O(9)-N(5)	1.276(6)	O(1)-N(3)	1.286(6)
O(2)-N(4)	1.291(7)	O(16)-N(6)	1.271(7)
Angles			
O(2)-Gd(1)-O(1)	83.90(15)	O(3)-Gd(1)-O(4)	72.19(17)
O(2)-Gd(1)-O(8)	69.66(17)	O(3)-Gd(1)-O(5)	72.79(18)
O(2)-Gd(1)-O(4)	70.53(17)	O(5)-Gd(1)-O(1)	133.75(16)
O(2)-Gd(1)-O(5)	137.67(17)	O(5)-Gd(1)-O(8)	74.41(17)
O(7)-Gd(1)-O(2)	115.75(16)	O(5)-Gd(1)-O(4)	133.12(17)
O(7)-Gd(1)-O(1)	69.90(15)	O(11)-Cu(2)-O(11)#1	180.0
O(7)-Gd(1)-O(8)	73.05(18)	O(11)-Cu(2)-O(10)#1	87.50(17)
O(7)-Gd(1)-O(4)	137.69(16)	O(11)#1-Cu(2)-O(10)	87.50(17)
O(7)-Gd(1)-O(5)	72.57(17)	O(11)#1-Cu(2)-O(10)#1	92.50(17)
O(6)-Gd(1)-O(2)	84.83(16)	O(11)-Cu(2)-O(10)	92.49(17)
O(6)-Gd(1)-O(7)	142.93(18)	O(10)-Cu(2)-O(10)#1	180.0
O(6)-Gd(1)-O(1)	146.16(17)	O(12)-Cu(1)-O(13)	88.36(18)
O(6)-Gd(1)-O(8)	87.60(18)	O(12)-Cu(1)-N(1)	92.30(19)
O(6)-Gd(1)-O(4)	76.79(18)	O(14)-Cu(1)-O(12)	162.47(19)
O(6)-Gd(1)-O(3)	88.10(17)	O(14)-Cu(1)-O(15)	90.81(19)
O(6)-Gd(1)-O(5)	71.87(18)	O(14)-Cu(1)-O(13)	109.13(18)
O(8)-Gd(1)-O(1)	117.73(15)	O(14)-Cu(1)-N(1)	87.8(2)
O(8)-Gd(1)-O(4)	138.25(18)	O(15)-Cu(1)-O(12)	87.03(19)
O(4)-Gd(1)-O(1)	69.38(15)	O(15)-Cu(1)-O(13)	93.0(2)
O(3)-Gd(1)-O(2)	142.69(18)	O(15)-Cu(1)-N(1)	173.3(2)
O(3)-Gd(1)-O(7)	91.24(17)	N(1)-Cu(1)-O(13)	93.66(19)
O(3)-Gd(1)-O(1)	81.91(16)	N(4)-O(2)-Gd(1)	141.9(4)
O(3)-Gd(1)-O(8)	146.62(18)	N(3)-O(1)-Gd(1)	139.2(4)

Symmetry transformations used to generate equivalent atoms: #1 -x+1,-y+1,-z+1

Table S5. Selected bond lengths [Å] and angles [°] for **2**

Bond distances			
Dy(1)-O(2)	2.328(4)	Cu(2)-O(11)	1.928(4)
Dy(1)-O(7)	2.325(5)	Cu(2)-O(11)#1	1.928(4)
Dy(1)-O(1)	2.453(4)	Cu(2)-O(10)	1.933(4)
Dy(1)-O(6)	2.301(5)	Cu(2)-O(10)#1	1.933(4)
Dy(1)-O(8)	2.356(5)	Cu(1)-O(12)	1.964(4)
Dy(1)-O(4)	2.362(5)	Cu(1)-O(14)	1.934(4)
Dy(1)-O(3)	2.306(5)	Cu(1)-O(15)	1.947(5)
Dy(1)-O(5)	2.368(5)	Cu(1)-O(13)	2.206(4)
O(2)-N(4)	1.289(7)	O(1)-N(3)	1.294(6)
O(9)-N(5)	1.272(6)	O(16)-N(6)	1.275(7)
Angles			
O(2)-Dy(1)-O(1)	84.19(15)	O(3)-Dy(1)-O(1)	81.39(16)
O(2)-Dy(1)-O(8)	70.40(17)	O(3)-Dy(1)-O(8)	145.95(17)
O(2)-Dy(1)-O(4)	70.04(17)	O(3)-Dy(1)-O(4)	72.74(17)
O(2)-Dy(1)-O(5)	137.96(16)	O(3)-Dy(1)-O(5)	72.56(17)
O(7)-Dy(1)-O(2)	116.33(16)	O(5)-Dy(1)-O(1)	133.32(16)
O(7)-Dy(1)-O(1)	69.72(15)	O(11)#1-Cu(2)-O(11)	180.0
O(7)-Dy(1)-O(8)	73.05(17)	O(11)#1-Cu(2)-O(10)#1	92.31(18)
O(7)-Dy(1)-O(4)	137.39(17)	O(11)-Cu(2)-O(10)#1	87.69(18)
O(7)-Dy(1)-O(5)	72.37(17)	O(11)-Cu(2)-O(10)	92.31(18)
O(6)-Dy(1)-O(2)	84.25(16)	O(11)#1-Cu(2)-O(10)	87.69(18)
O(6)-Dy(1)-O(7)	143.80(17)	O(10)-Cu(2)-O(10)#1	180.0
O(6)-Dy(1)-O(1)	145.35(17)	O(12)-Cu(1)-O(13)	88.49(18)
O(6)-Dy(1)-O(8)	88.26(18)	O(14)-Cu(1)-O(12)	161.67(19)
O(6)-Dy(1)-O(4)	76.12(18)	O(14)-Cu(1)-O(15)	91.1(2)
O(6)-Dy(1)-O(3)	88.44(18)	O(14)-Cu(1)-O(13)	109.82(19)
O(6)-Dy(1)-O(5)	72.78(18)	O(14)-Cu(1)-N(1)	87.5(2)
O(8)-Dy(1)-O(1)	118.02(16)	O(15)-Cu(1)-O(12)	87.1(2)
O(8)-Dy(1)-O(4)	138.59(17)	O(15)-Cu(1)-O(13)	92.6(2)
O(8)-Dy(1)-O(5)	74.10(16)	O(15)-Cu(1)-N(1)	174.1(2)
O(4)-Dy(1)-O(1)	69.23(16)	N(1)-Cu(1)-O(12)	92.4(2)
O(4)-Dy(1)-O(5)	133.38(18)	N(1)-Cu(1)-O(13)	93.2(2)
O(3)-Dy(1)-O(2)	142.75(17)	N(4)-O(2)-Dy(1)	142.2(4)
O(3)-Dy(1)-O(7)	90.35(17)	N(3)-O(1)-Dy(1)	138.9(4)

Symmetry transformations used to generate equivalent atoms: #1 -x+1,-y+1,-z+1

Table S6. Selected bond lengths [Å] and angles [°] for **3**.

Bond distances			
Y-O(5)	2.370(6)	Cu(1)-O(9)#1	1.935(5)
Y-O(1)	2.359(6)	Cu(1)-O(9)	1.935(5)
Y-O(7)	2.377(5)	Cu(1)-O(10)#1	1.938(5)
Y-O(11)	2.350(5)	Cu(1)-O(10)	1.938(5)
Y-O(6)	2.341(6)	Cu(2)-O(14)	1.936(6)
Y-O(2)	2.288(5)	Cu(2)-O(14)#2	1.936(6)
Y-O(4)	2.339(6)	Cu(2)-O(13)	1.905(7)
Y-O(3)	2.333(6)	Cu(2)-O(13)#2	1.905(7)
O(7)-N(1)	1.300(8)	Cu(3)-O(15)	1.903(7)
O(8)-N(2)	1.277(8)	Cu(3)-O(18)	1.943(7)
O(11)-N(3)	1.294(8)	Cu(3)-O(16)	2.193(7)
O(12)-N(4)	1.295(9)	Cu(3)-O(17)	1.961(6)
Angles			
O(5)-Y-O(7)	119.07(19)	O(3)-Y-O(6)	143.3(2)
O(1)-Y-O(5)	136.5(2)	O(3)-Y-O(4)	72.2(2)
O(1)-Y-O(7)	71.33(19)	O(15)-Cu(3)-O(18)	171.3(3)
O(11)-Y-O(5)	71.2(2)	O(15)-Cu(3)-O(16)	91.1(3)
O(11)-Y-O(1)	69.00(19)	O(15)-Cu(3)-O(17)	86.6(3)
O(11)-Y-O(7)	81.40(19)	O(15)-Cu(3)-N(6)	90.3(3)
O(6)-Y-O(5)	72.6(2)	O(18)-Cu(3)-O(16)	97.2(3)
O(6)-Y-O(1)	141.06(19)	O(18)-Cu(3)-O(17)	90.0(3)
O(6)-Y-O(7)	70.95(18)	O(18)-Cu(3)-N(6)	90.9(3)
O(6)-Y-O(11)	114.03(19)	O(17)-Cu(3)-O(16)	95.4(3)
O(2)-Y-O(5)	145.7(2)	O(17)-Cu(3)-N(6)	165.2(3)
O(2)-Y-O(1)	73.3(2)	N(6)-Cu(3)-O(16)	99.1(3)
O(2)-Y-O(7)	82.52(18)	O(9)#1-Cu(1)-O(9)	180
O(2)-Y-O(11)	142.0(2)	O(9)#1-Cu(1)-O(10)	92.8(2)
O(2)-Y-O(6)	92.6(2)	O(9)-Cu(1)-O(10)#1	92.8(2)
O(2)-Y-O(4)	73.4(2)	O(9)#1-Cu(1)-O(10)#1	87.2(2)
O(2)-Y-O(3)	81.5(2)	O(9)-Cu(1)-O(10)	87.2(2)
O(4)-Y-O(5)	72.6(2)	O(10)#1-Cu(1)-O(10)	180.0
O(4)-Y-O(1)	133.6(2)	O(14)#2-Cu(2)-O(14)	180.0
O(4)-Y-O(7)	133.81(19)	O(13)#2-Cu(2)-O(14)	93.2(3)
O(4)-Y-O(11)	139.1(2)	O(13)#2-Cu(2)-O(14)#2	86.8(3)
O(4)-Y-O(6)	71.39(19)	O(13)-Cu(2)-O(14)	86.8(3)
O(3)-Y-O(5)	92.2(2)	O(13)-Cu(2)-O(14)#2	93.2(3)
O(3)-Y-O(1)	71.7(2)	O(13)-Cu(2)-O(13)#2	180.0
O(3)-Y-O(7)	142.5(2)	N(1)-O(7)-Y	140.2(4)
O(3)-Y-O(11)	90.9(2)	N(3)-O(11)-Y	143.3(5)

Symmetry transformations used to generate equivalent atoms: #1 -x+2,-y+1,-z, #2 -x+2,-y+1,-z+1

Table S7. Selected bond lengths [Å] and angles [°] for **4**.

Bond distances			
Dy(1)-O(5)	2.361(7)	Cu(1)-O(9)#1	1.929(7)
Dy(1)-O(1)	2.360(7)	Cu(1)-O(9)	1.929(7)
Dy(1)-O(7)	2.386(6)	Cu(1)-O(10)#1	1.935(6)
Dy(1)-O(11)	2.348(7)	Cu(1)-O(10)	1.935(6)
Dy(1)-O(6)	2.333(7)	Cu(2)-O(14)	1.932(9)
Dy(1)-O(2)	2.298(7)	Cu(2)-O(14)#2	1.932(9)
Dy(1)-O(4)	2.348(7)	Cu(2)-O(13)	1.938(10)
Dy(1)-O(3)	2.337(8)	Cu(2)-O(13)#2	1.938(10)
O(7)-N(1)	1.271(10)	Cu(3)-O(15)	1.919(9)
O(8)-N(2)	1.272(10)	Cu(3)-O(18)	1.937(11)
O(11)-N(3)	1.284(10)	Cu(3)-O(16)	2.187(9)
O(12)-N(4)	1.290(12)	Cu(3)-O(17)	1.956(8)
Angles			
O(5)-Dy(1)-O(7)	119.0(2)	O(3)-Dy(1)-O(11)	91.2(3)
O(1)-Dy(1)-O(5)	136.7(3)	O(3)-Dy(1)-O(4)	72.0(3)
O(1)-Dy(1)-O(7)	71.7(2)	O(15)-Cu(3)-O(18)	171.4(4)
O(11)-Dy(1)-O(5)	70.8(2)	O(15)-Cu(3)-O(16)	91.4(4)
O(11)-Dy(1)-O(1)	69.5(2)	O(15)-Cu(3)-O(17)	86.1(4)
O(11)-Dy(1)-O(7)	82.2(2)	O(15)-Cu(3)-N(6)	90.3(4)
O(11)-Dy(1)-O(4)	138.8(2)	O(18)-Cu(3)-O(16)	96.6(4)
O(6)-Dy(1)-O(5)	73.0(3)	O(18)-Cu(3)-O(17)	89.8(4)
O(6)-Dy(1)-O(1)	140.4(2)	O(18)-Cu(3)-N(6)	91.6(4)
O(6)-Dy(1)-O(7)	69.9(2)	O(17)-Cu(3)-O(16)	96.4(3)
O(6)-Dy(1)-O(11)	113.8(2)	O(17)-Cu(3)-N(6)	164.7(4)
O(6)-Dy(1)-O(4)	71.7(2)	N(6)-Cu(3)-O(16)	98.6(3)
O(6)-Dy(1)-O(3)	143.5(2)	O(9)-Cu(1)-O(9)#1	180.0(5)
O(2)-Dy(1)-O(5)	146.0(2)	O(9)-Cu(1)-O(10)#1	93.1(3)
O(2)-Dy(1)-O(1)	72.7(2)	O(9)#1-Cu(1)-O(10)	93.1(3)
O(2)-Dy(1)-O(7)	82.4(2)	O(9)#1-Cu(1)-O(10)#1	86.9(3)
O(2)-Dy(1)-O(11)	141.9(2)	O(9)-Cu(1)-O(10)	86.9(3)
O(2)-Dy(1)-O(6)	92.9(3)	O(10)#1-Cu(1)-O(10)	180.0(4)
O(2)-Dy(1)-O(4)	73.6(2)	O(14)#2-Cu(2)-O(14)	180.0(3)
O(2)-Dy(1)-O(3)	80.8(3)	O(14)#2-Cu(2)-O(13)#2	86.9(4)
O(4)-Dy(1)-O(5)	72.6(2)	O(14)-Cu(2)-O(13)	86.9(4)
O(4)-Dy(1)-O(1)	133.7(2)	O(14)-Cu(2)-O(13)#2	93.1(4)
O(4)-Dy(1)-O(7)	133.1(3)	O(14)#2-Cu(2)-O(13)	93.1(4)
O(3)-Dy(1)-O(5)	92.3(3)	O(13)-Cu(2)-O(13)#2	180.0(3)
O(3)-Dy(1)-O(1)	72.0(3)	N(1)-O(7)-Dy(1)	141.3(5)
O(3)-Dy(1)-O(7)	143.1(2)	N(3)-O(11)-Dy(1)	144.3(6)

Symmetry transformations used to generate equivalent atoms: #1 x+2,y+1,z, #2 x+2,y+1,z+1

Table S8. Selected bond lengths [Å] and angles [°] for **5**.

Bond distances			
Tb-O(5)	2.363(5)	Cu(1)-O(9)#1	1.911(5)
Tb-O(1)	2.372(5)	Cu(1)-O(9)	1.911(5)
Tb-O(7)	2.394(5)	Cu(1)-O(10)	1.935(5)
Tb-O(11)	2.369(5)	Cu(1)-O(10)#1	1.935(5)
Tb-O(6)	2.349(5)	Cu(2)-O(14)#2	1.930(6)
Tb-O(2)	2.303(5)	Cu(2)-O(14)	1.930(6)
Tb-O(4)	2.349(6)	Cu(2)-O(13)#2	1.923(6)
Tb-O(3)	2.340(5)	Cu(2)-O(13)	1.921(6)
O(7)-N(1)	1.284(7)	Cu(3)-O(15)	1.921(6)
O(8)-N(2)	1.285(7)	Cu(3)-O(18)	1.934(7)
O(11)-N(3)	1.285(8)	Cu(3)-O(16)	2.182(6)
O(12)-N(4)	1.292(8)	Cu(3)-O(17)	1.964(6)
Angles			
O(5)-Tb-O(1)	136.92(18)	O(3)-Tb-O(6)	142.94(19)
O(5)-Tb-O(7)	119.04(17)	O(3)-Tb-O(4)	71.75(19)
O(5)-Tb-O(11)	71.46(18)	O(15)-Cu(3)-O(18)	171.2(3)
O(1)-Tb-O(7)	71.40(16)	O(15)-Cu(3)-O(16)	90.7(3)
O(11)-Tb-O(1)	69.12(17)	O(15)-Cu(3)-O(17)	86.6(3)
O(11)-Tb-O(7)	81.61(17)	O(15)-Cu(3)-N(6)	90.4(2)
O(6)-Tb-O(5)	72.61(19)	O(18)-Cu(3)-O(16)	97.5(3)
O(6)-Tb-O(1)	140.70(17)	O(18)-Cu(3)-O(17)	89.6(3)
O(6)-Tb-O(7)	70.59(16)	O(18)-Cu(3)-N(6)	91.4(3)
O(6)-Tb-O(11)	114.25(17)	O(17)-Cu(3)-O(16)	95.5(3)
O(2)-Tb-O(5)	145.73(18)	O(17)-Cu(3)-N(6)	165.3(3)
O(2)-Tb-O(1)	72.95(18)	N(6)-Cu(3)-O(16)	98.9(3)
O(2)-Tb-O(7)	82.27(16)	O(9)#1-Cu(1)-O(9)	180.0
O(2)-Tb-O(11)	141.79(18)	O(9)-Cu(1)-O(10)	86.9(2)
O(2)-Tb-O(6)	92.36(18)	O(9)-Cu(1)-O(10)#1	93.1(2)
O(2)-Tb-O(4)	73.43(18)	O(9)#1-Cu(1)-O(10)#1	86.92)
O(2)-Tb-O(3)	81.03(18)	O(9)#1-Cu(1)-O(10)	93.1(2)
O(4)-Tb-O(5)	72.59(18)	O(10)-Cu(1)-O(10)#1	180.00(17)
O(4)-Tb-O(1)	133.43(18)	O(14)-Cu(2)-O(14)#2	180.0(4)
O(4)-Tb-O(7)	133.46(19)	O(13)-Cu(2)-O(14)	87.0(3)
O(4)-Tb-O(11)	139.34(19)	O(13)#2-Cu(2)-O(14)#	87.0(3)
O(4)-Tb-O(6)	71.41(18)	O(13)#2-Cu(2)-O(14)	93.0(3)
O(3)-Tb-O(5)	92.53(18)	O(13)-Cu(2)-O(14)#2	93.0(3)
O(3)-Tb-O(1)	71.98(18)	O(13)-Cu(2)-O(13)#2	180.0(2)
O(3)-Tb-O(7)	142.79(18)	N(1)-O(7)-Tb	140.1(4)
O(3)-Tb-O(11)	91.46(18)	N(3)-O(11)-Tb	142.6(5)

Symmetry transformations used to generate equivalent atoms: #1 -x+2,-y+1,-z, #2 -x+2,-y+1,-z+1

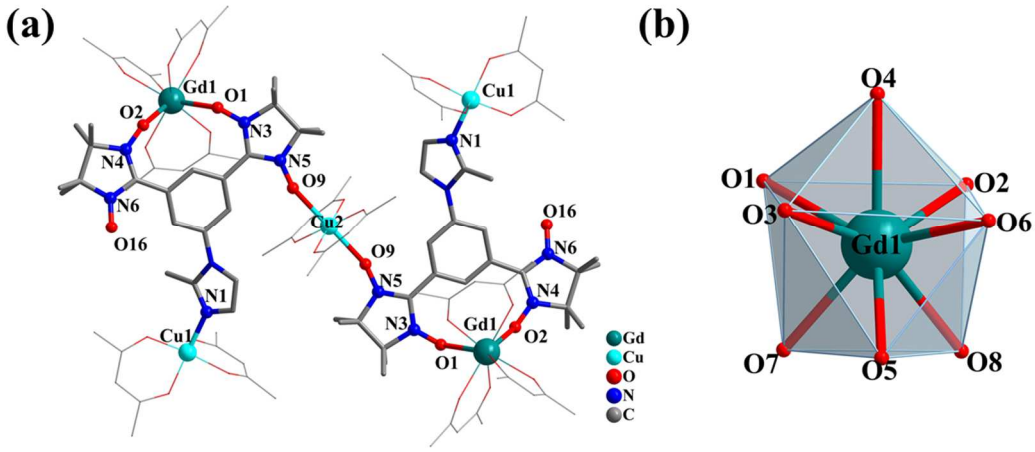

Figure S1. (a) The pentanuclear structure of **1** (H and F atoms are omitted for clarity). (b) The coordination polyhedron of Gd^{III} ion

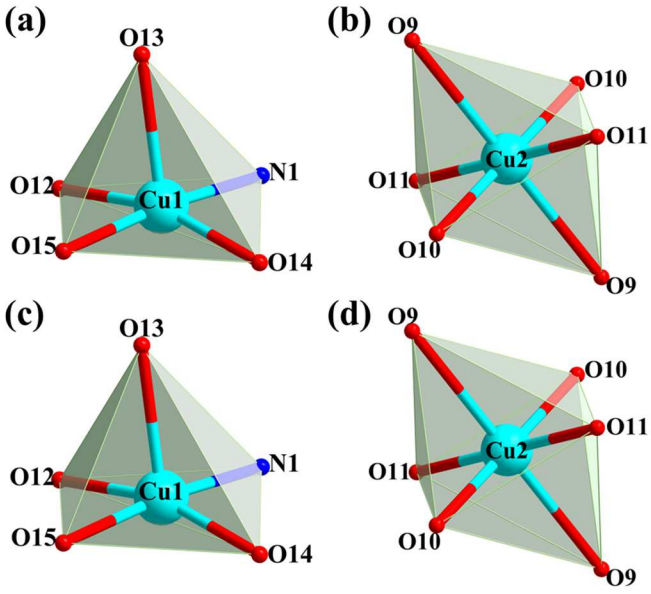

Figure S2. Coordination polyhedrons of Cu1 ion (a) and Cu2 ion (b) in **1** and Cu1 ion (c) and Cu2 ion (d) in complex **2**.

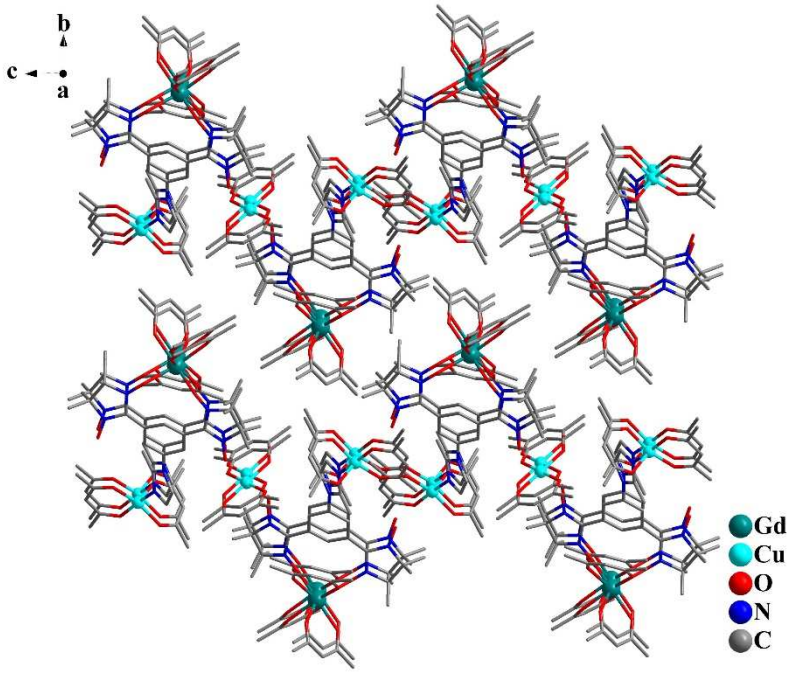

Figure S3. Crystal packing diagram of **1** (H and F atoms are omitted).

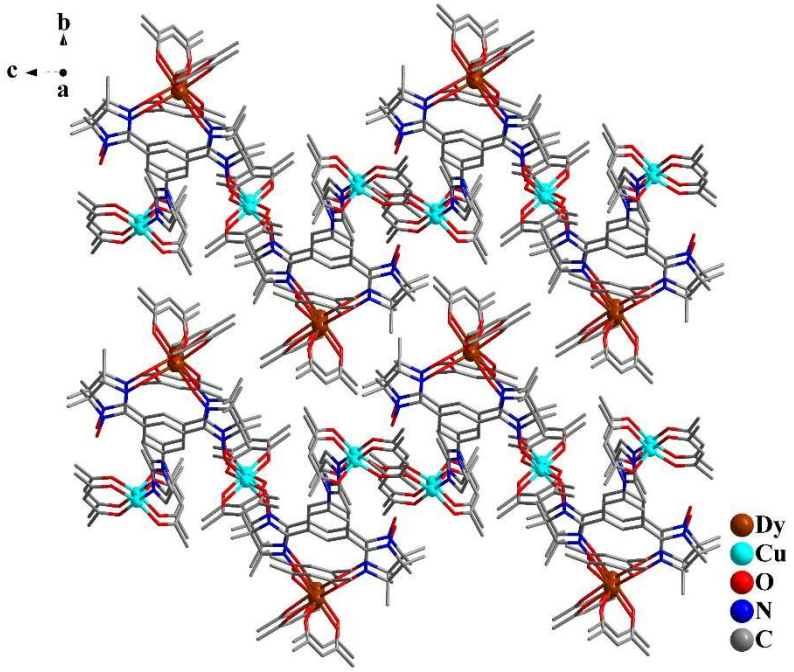

Figure S4. Crystal packing diagram of **2** (H and F atoms are omitted).

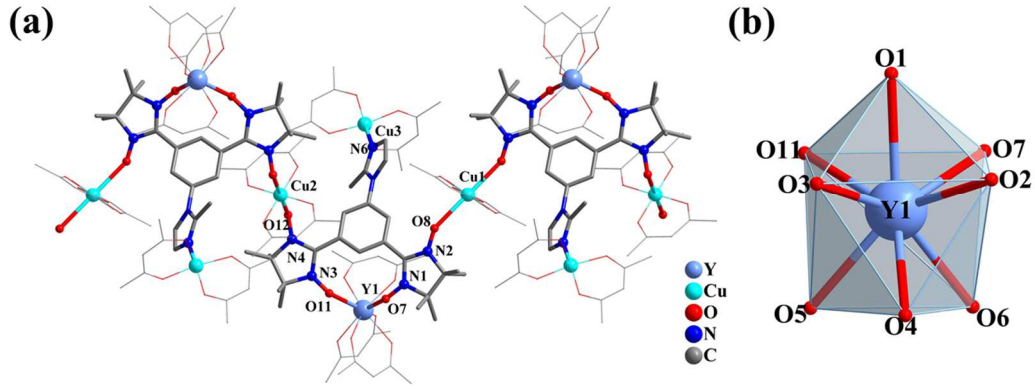

Figure S5. (a) One-dimensional structure of **3** (H and F atoms are omitted for clarity). (b) The coordination polyhedron of Y^{III} ion.

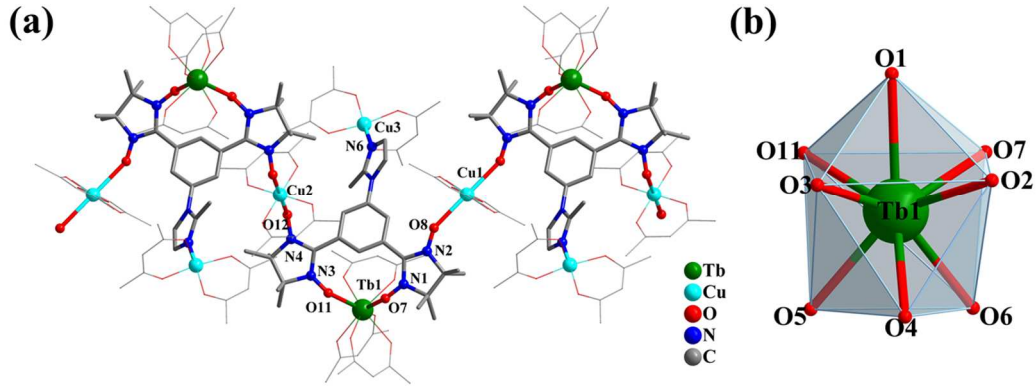

Figure S6. (a) One-dimensional structure of **5** (H and F atoms are omitted for clarity). (b) The coordination polyhedron of Tb^{III} ion.

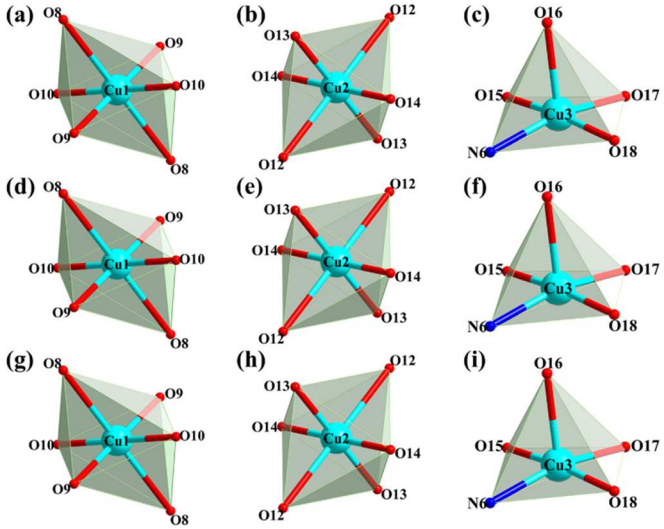

Figure S7. Coordination polyhedrons of Cu1 ion (a), Cu2 ion (b) and Cu3 ion (c) in **3**, Cu1 ion

(d), Cu2 ion (e) and Cu3 ion (f) in **4** and Cu1 ion (g), Cu2 ion (h) and Cu3 ion (i) in complex **5**.

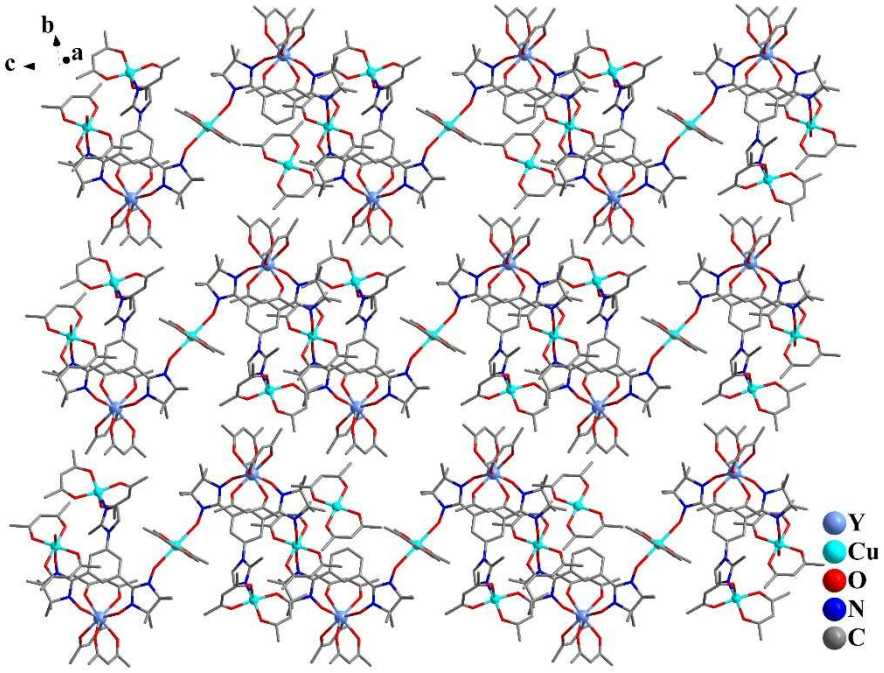

Figure S8. Crystal packing diagram of **3** (H and F atoms are omitted).

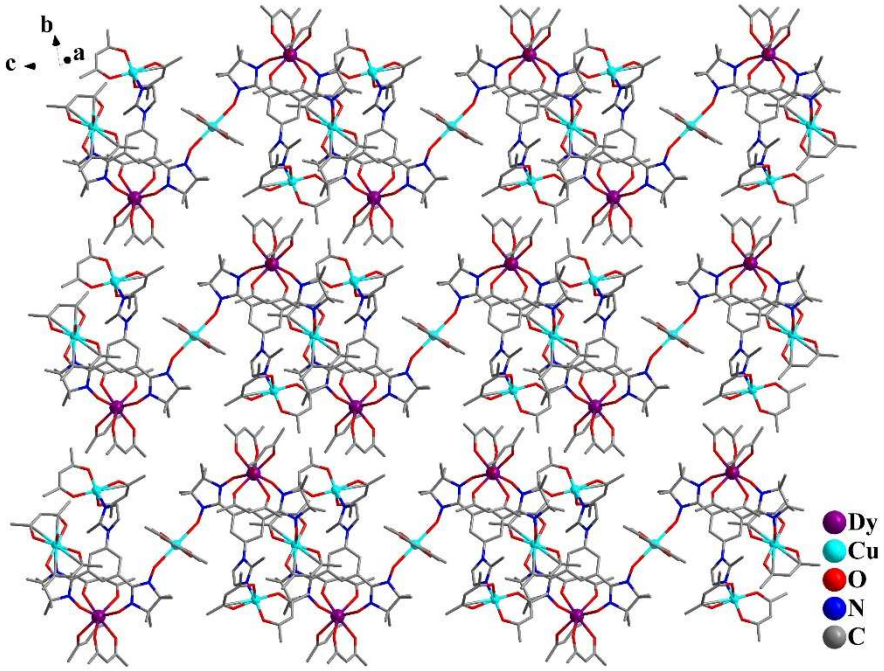

Figure S9. Crystal packing diagram of **4** (H and F atoms are omitted).

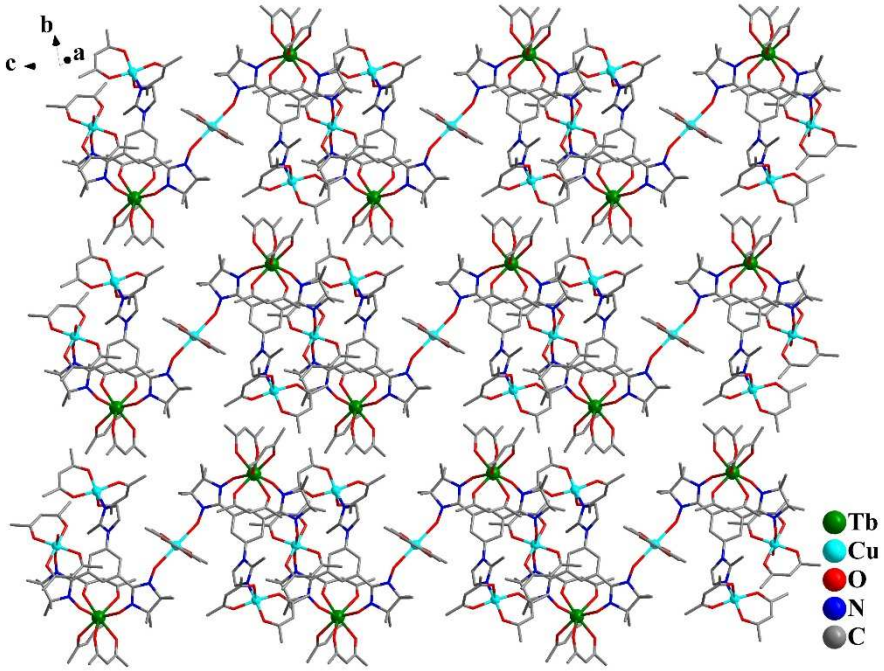

Figure S10. Crystal packing diagram of **5** (H and F atoms are omitted).

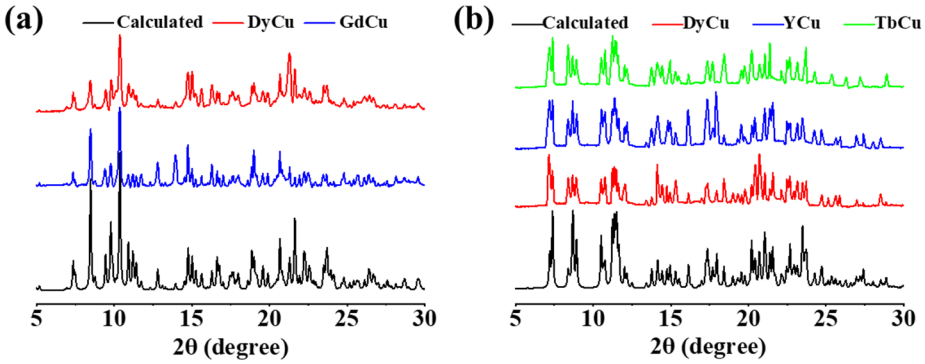

Figure S11. Powder X-ray diffraction patterns of **1-2** (a) and **3-5** (b).

.

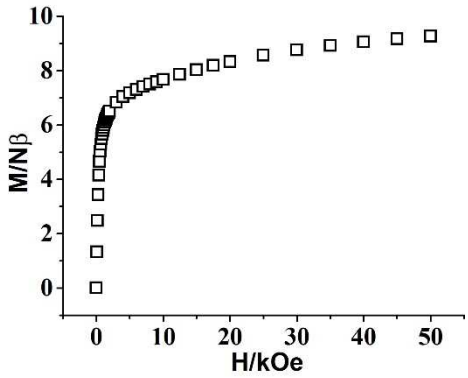

Figure S12. M versus H plot for **4** at 2 K.

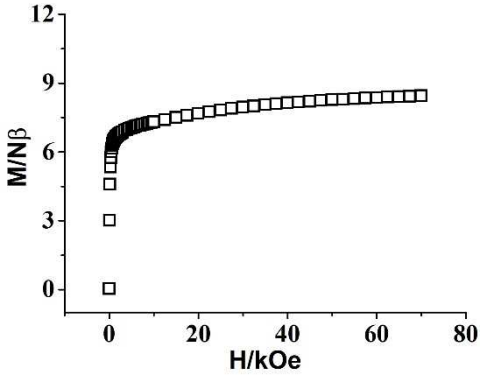

Figure S13. M versus H plot for **5** at 2 K.

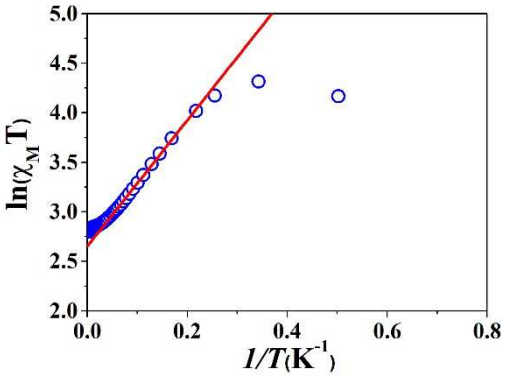

Figure S14. $\ln(\chi_M T)$ versus T^{-1} plot of **4** (the solid line represents the linear fit between 4.6 and 19 K).

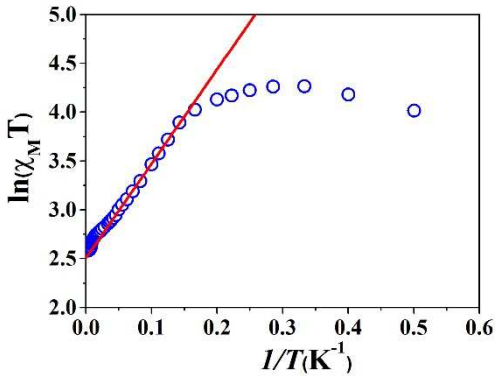

Figure S15. ln(χ_MT) versus T^{-1} plot of **5** (the solid red line represents the linear fit between 7 and 22 K).

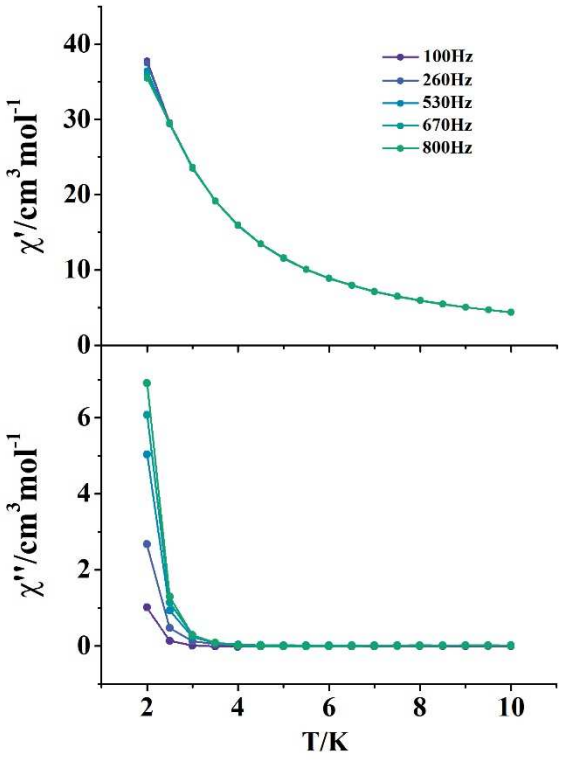

Figure S16. Temperature-dependent ac signals without dc field for **2**.

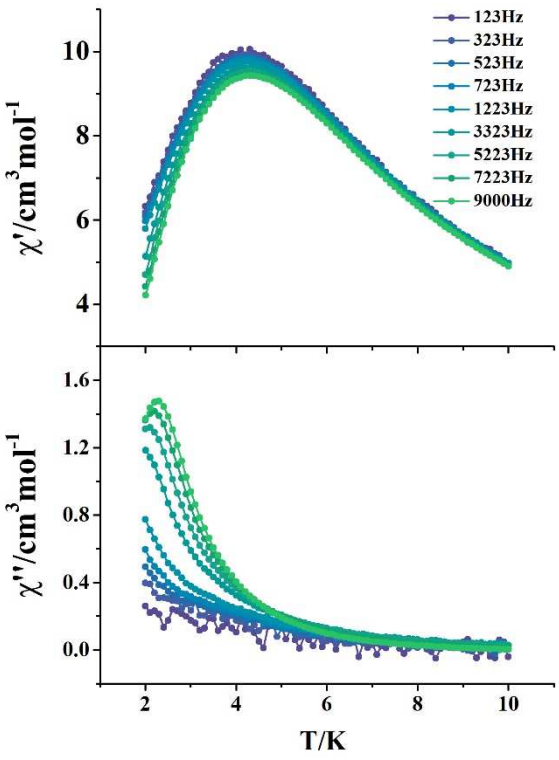

Figure S17. Temperature-dependent ac signals under 3000 Oe dc field for **2**.

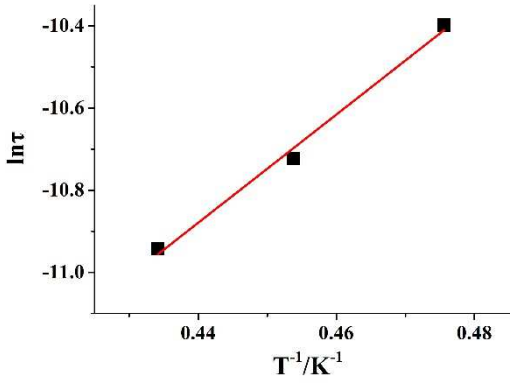

Figure S18. The lnτ vs. 1/T plots (red-line: fitting results by the Arrhenius law) for **2**

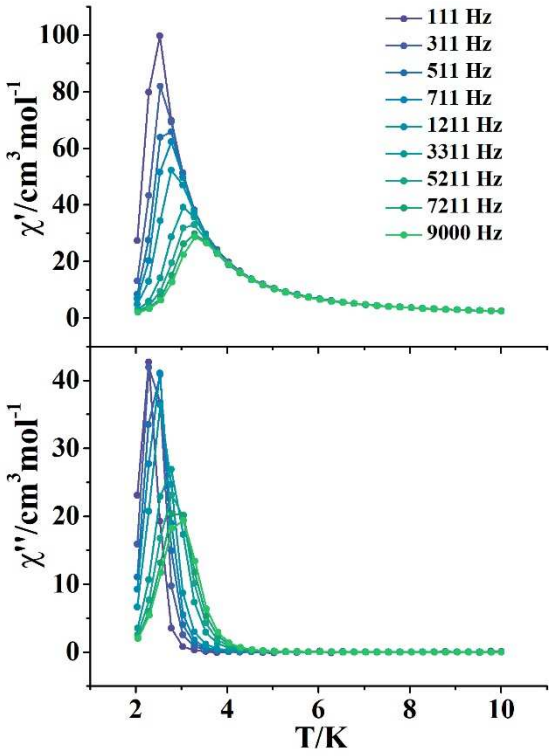

Figure S19. Temperature-dependent ac signals without dc field for **4**.

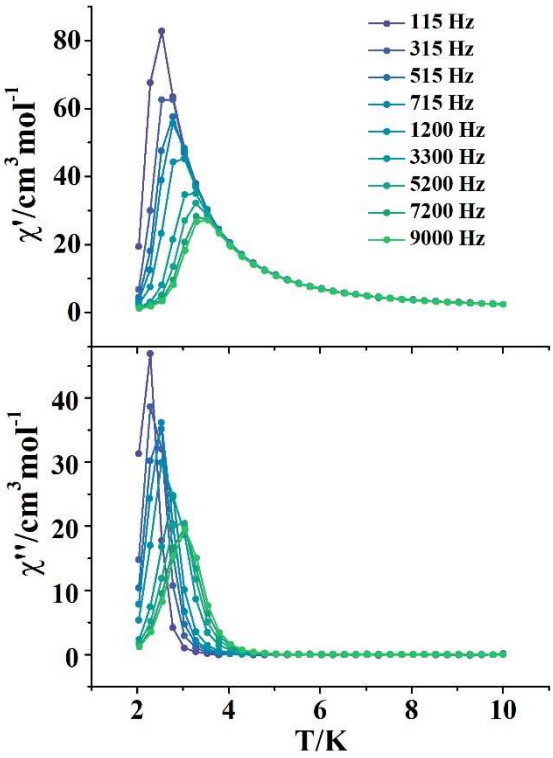

Figure S20. Temperature-dependent ac signals without dc field for **5**.